

The Optical – Infrared Colors of CORALS QSOs: Searching for Dust Reddening Associated With High Redshift Damped Lyman Alpha Systems¹

Sara L. Ellison

*University of Victoria, Dept. Physics & Astronomy, Elliott Building, 3800 Finnerty Rd,
Victoria, V8P 1A1, British Columbia, Canada*

sarae@uvic.ca

Patrick B. Hall

*Department of Physics and Astronomy, York University, 4700 Keele St., Toronto, Ontario
M3J 1P3, Canada*

phall@yorku.ca

Paulina Lira

Departamento de Astronomía, Universidad de Chile, Casilla 36-D, Santiago, Chile

plira@das.uchile.cl

ABSTRACT

The presence of dust in quasar absorbers, such as damped Lyman alpha (DLA) systems, may cause the background QSO to appear reddened. We investigate the extent of this potential reddening by comparing the optical-to-infrared (IR) colors of QSOs with and without intervening absorbers. Our QSO sample is based on the Complete Optical and Radio Absorption Line System (CORALS) survey of Ellison et al (2001). The CORALS dataset consists of 66 radio-selected QSOs at $z_{\text{em}} \geq 2.2$ with complete optical identifications. We have obtained near-simultaneous B and K band magnitudes for subset of the CORALS sample and supplemented our observations with further measurements published in the literature. In total, we have B–K colors for 42/66 QSOs of which 14 have intervening DLAs. To account for redshift-related color changes, the B–K colors are normalized using the Sloan Digital Sky Survey (SDSS) QSO composite. The mean normalized B–K color of the DLA sub-sample is +0.12, whereas the mean for the no-DLA sample is –0.10; both distributions have RMS scatters ~ 0.5 .

Neither a student’s T-test nor a KS test indicate that there is any significant difference between the two color distributions. Based on simulations which redden the colors of QSOs with intervening DLAs, we determine a reddening limit which corresponds to $E(B - V) < 0.04$ (SMC-like extinction) at 99% confidence (3σ), assuming that $E(B - V)$ is the same for all DLAs. Finally, we do not find any general correlation between absorber properties (such as $[\text{Fe}/\text{Zn}]$ or neutral hydrogen column density) and B–K color. The two reddest QSOs with DLAs in our sample have HI column densities which differ from each other by an order of magnitude and moderate gas-to-dust ratios as inferred from chemical abundances. One of these two QSOs shows evidence for strong associated absorption from X-ray observations, an alternative explanation for its very red color. We conclude that the presence of intervening galaxies causes a minimal reddening of the background QSO.

Subject headings: ISM:general, galaxies:high-redshift, quasars:absorption lines, dust, extinction

1. Introduction

1.1. Red Quasars

Although quasars are usually regarded as objects which are characterised by an ultra-violet (UV) excess, the existence of red QSOs has been known for more than two decades (e.g. Smith & Spinrad 1980; Bregman et al 1981; Stein & Sitko 1984). Despite their long history, red QSOs have continued to attract much interest in the literature, most notably the on-going debate to identify the primary cause of their extreme optical–infrared (IR) colors. Probably the most popular explanation for red QSOs is extinction due to dust at the systemic redshift, a conclusion that is gaining substantial support from the current generation of large QSO surveys (e.g. Richards et al. 2003; Hopkins et al. 2004; Glikman et al 2004; White et al. 2003). There are also convincing examples of individual QSOs which appear to have been highly reddened due to local (to the QSO) dust (e.g. Rawlings et al. 1995; Gregg et al. 2000; Stern et al. 2003). If dust is indeed a common ingredient in QSOs, the corollary is that samples based on optically selected sources could potentially miss the reddened population, whereas radio-selected quasars would represent a more complete sample (e.g. Webster et al

¹These data were obtained from the NTT on La Silla (ESO program 072.A-0014(A, B, C, D))

1995; Barkhouse & Hall 2001). Indeed, Webster et al. (1995) have claimed that up to 80% of QSOs may be hidden from the eyes of optical surveys due to dust extinction.

However, some observations do not support the hypothesis of dust local to the QSO as the cause of reddening. For example, millimetre observations (Drinkwater, Wiklind & Combes 1996) of 11 of the reddest Webster et al. (1995) sources failed to detect CO which argues against the presence of host galaxy dust in these cases. Other possible sources of QSO ‘reddening’ include the effect of host galaxy starlight and synchrotron radiation (Francis, Whiting & Webster 2000; Whiting, Webster & Francis, 2001; Benn et al. 1998).

1.2. Dust Reddening Associated with Intervening Galaxies

One factor that could have a significant impact on reddening QSO light that remains relatively unexplored is the presence of intervening dust located in foreground galaxies. The identification of a handful of red lensed QSOs lends credibility to this scenario, in which dust in the lensing galaxy reddens the background source (e.g. Gregg et al. 2000; Falco et al. 1999, Wucknitz et al 2003). The issue of dusty intervening galaxies is of interest not only in order to assess its contribution to the red QSO population, but is also of crucial importance for the study of quasar absorption lines. Quasar absorbers, such as the damped Lyman alpha (DLA) systems which correspond to the signatures of high redshift galaxies imprinted on the continuum of a background QSO, represent one of our best tools for studying the early galaxy population. Previous surveys for DLAs have almost universally relied on large optical databases of QSOs to find intervening absorbers. Since only relatively bright, optically selected QSOs have been used to identify DLAs, there has been widespread concern that dusty intervening galaxies may obscure the background QSO so that it drops below the survey magnitude limit. Such a selection effect would result in a biased view of high redshift galaxies. This general concern has been quantified in a number of theoretical works which have attempted to estimate the amount of reddening that a QSO may suffer and consequently what fraction of the DLA population, and their contribution towards the cosmic gas and metals budget, may have been overlooked (e.g. Fall & Pei 1993; Pei & Fall 1995; Pei, Fall & Hauser 1998; Churches et al. 2004; Vladilo & Péroux, 2005). However, until recently there had been little observational progress in quantifying the number of missed DLAs due to extinction effects.

The first systematic program to quantify dust bias was undertaken by Ellison et al. (2001) by searching for DLAs in an optically complete radio-selected sample of QSOs. The Complete Optical and Radio Absorption Line System (CORALS) survey was based on a homogeneous sample of 66 radio-selected, flat spectrum QSOs taken from the Parkes catalogue,

complete down to 0.25 Jy. Extensive optical follow-up observations resulted in identifications for *all* sources. Therefore, subsequent spectroscopic searches for DLAs were based on a complete sample, ideal for determining the extent to which intervening galaxies obscure background QSOs. Ellison et al. (2001) determined that the neutral gas mass density of DLAs (Ω_{DLA}) may have been previously under-estimated by at most a factor of ~ 2 . However, this work also found tentative evidence that Ω_{DLA} and $n(z)$ (the DLA number density) may be under-estimated for bright QSO samples with magnitude limits $B \lesssim 19.5$. Ellison et al. (2004) re-visited this issue and suggested that this could be understood in terms of an Eddington bias if the optical luminosity function deviates from a simple power law. To extend the original CORALS sample to lower redshifts, Ellison et al. (2004) studied Mg II absorption systems in an analogous radio-selected QSO sample. The main conclusion of that work was that the number density of intervening systems selected via Mg II absorption in the range $0.6 < z < 1.7$ is in excellent agreement with magnitude limited samples (e.g. Nestor, Turnshek & Rao 2005). Most recently, Akerman et al. (2005) have measured the metal abundances of $z > 1.8$ CORALS DLAs and found that the weighted mean metallicity based on zinc (an undepleted proxy for Fe) is only marginally higher (but consistent within the error bars) than previous samples.

Although the results from CORALS indicate that magnitude limited surveys (at least those complete to $B \sim 19$) have not missed a significant fraction of the gas or metals budget, this is not to say that DLAs are dust-free. In fact, it has been known for over a decade, based on the ratios of refractory and non-refractory elements, that dust is present in DLAs (Meyer & Roth 1990; Meyer & York 1992; Pettini et al. 1994, 1997). Understanding the level of extinction caused by this dust has so far yielded conflicting results. For example, Fall, Pei & McMahon (1989) and Pei, Fall & Bechtold (1991) found a significant difference between the spectral indices of QSOs with intervening DLAs and a control sample. However, this result has not been reproduced with larger, homogeneous QSO samples. Currently, the most stringent limit for reddening due to intervening DLAs has been obtained from fitting spectral indices to ~ 1450 QSOs from the Sloan Digital Sky Survey (SDSS): $E(B - V) < 0.02$ for SMC-like extinction (Murphy & Liske 2004). Despite this sensitive limit, studies of spectral indices suffer from two drawbacks: they utilize limited wavelength coverage in the optical regime and have not yet been conducted on unbiased samples (i.e. they were taken from magnitude limited surveys).

1.3. Optical–Infrared Colors and Extinction Curves

In this work, we take a different approach to studying the effect of dust extinction from intervening DLAs by using optical–IR QSO colors to search for a reddening signature. This technique has the advantage of using a wide wavelength baseline, from the observed frame B to K bands, over which to detect the effect of extinction. Moreover, by studying QSOs from the CORALS survey, we have a sample which is optically complete and in which all of the intervening high redshift DLAs have already been identified and metallicities measured.

The observed reddening obviously depends largely on the assumed extinction law, although the QSO and galaxy (i.e. dust) redshift also play a part (as we demonstrate below). Despite its ubiquity in astrophysical environments, the properties of dust remain relatively poorly understood (see reviews by Mathis 1990 and Draine 2003) and reliable empirical extinction data are available for only the Milky Way (MW) and Magellanic Clouds. In particular, data are sparse in the far-ultraviolet (FUV, Hutchings & Giasson 2001) and below the Lyman limit there is simply no flux with which to work. FUV wavelengths are particularly important for the present work, which considers the optical–IR colors of high redshift QSOs. The most often used parameterization of Galactic extinction is that of Cardelli, Clayton & Mathis (1989; hereafter CCM89). The advantage of the CCM89 formulae is that $\xi(\lambda) = A_\lambda/A_V$ can be calculated for any value of R_V ². Another popular parameterization of Galactic extinction is that of Pei (1992), although this is for a fixed value of $R_V = 3.08$. A comparison of these two extinction law fits is shown in Figure 1, with an $R_V = 3.08$ for the CCM89 law in order to match the Pei (1992) curve. It can be seen that at IR and optical wavelengths, the two curves are in close agreement. However, in the FUV ($\lambda < 1200 \text{ \AA}$) the curves diverge; this is purely due to extrapolation of the different fitting functions into a regime where no data were available. Whereas an extrapolation of the Pei (1992) parameterization leads to a flattening of $\xi(\lambda)$, the CCM89 curve rises quickly at FUV wavelengths. In Figure 1 we also show the extinction curves of the SMC and LMC as fitted by Pei (1992), again extrapolated to the FUV using the published fitting functions.

We illustrate the expected reddening due to intervening dust in Figures 2, 3 and 4. In each figure, we plot the theoretical reddening (as measured by a change in the B–K color) of a QSO at $z_{\text{em}} = 3$ as a function of $E(B - V)$. Since the color change depends on the redshift of the intervening dust, four different lines are plotted for dust at $z_{\text{dust}} = 2.0, 2.3, 2.6, 2.9$. The reddening induced by the two Galactic extinction curves is quite similar, although a CCM89 law produces slightly redder colors due to the rapid rise of $\xi(\lambda)$ in the FUV. Reddening is most severe for SMC type dust, and could be even more extreme if the true extinction law

²In the usual notation, $R_V = A_V/E(B - V)$, i.e. the total-to-selective extinction.

continues to rise at FUV wavelengths. That is, the parameterization of SMC dust by Pei (1992) may be considered conservative.

2. Observations and Data Reduction

Since flat spectrum radio-loud QSOs (RLQs) are highly variable, it is important to obtain optical and IR data from near-simultaneous epochs (e.g. Francis, Whiting & Webster 2000, hereafter FWW00). We achieved this by using the optical (SuSI2) and IR (SofI) imagers on the New Technology Telescope (NTT) at La Silla observatory. Since both instruments are mounted on the same Nasmyth platform, the overhead incurred by switching between them is typically only about 2 minutes, depending on the source position relative to the zenith. Our strategy was therefore to observe a sequence of QSOs in the optical and then change to the IR. Optical and IR photometric standard stars were observed throughout the night at airmasses up to 1.8.

Our data were obtained during two runs in October 2003 and March 2004. The March 2004 run experienced excellent conditions: photometric transparency and typical seeing ~ 0.6 arcsec. The earlier October 2003 run, suffered from somewhat poorer seeing (~ 1 arcsec) and the end of the last night (during which only SofI was used) was not photometric.

2.1. Optical Imaging

In addition to B-band images, we obtained supplemental V-band images for most QSOs with redshifts $z_{\text{em}} > 3.0$. Typical exposure times in the B and V bands ranged from 10 to 200 seconds (see Table 1), the total integration was divided between two exposures with a spatial offset of a few hundred pixels between exposures. We used SuSI2 in 2x2 binning mode which yielded a pixel scale of 0.16 arcsec/pixel. Standard IRAF procedures were used for the reduction of the optical data: a bias was constructed from a median combination of five frames and the overscan was fitted and subtracted interactively. The initial flat-fielding was executed using dome-flats to correct pixel-to-pixel variations, followed by an illumination correction of large-scale variations constructed from a super-sky flat. Instrumental magnitudes were determined for each night using IRAF's *gphot* package with between 20 and 40 standard stars taken from Landolt (1992). The photometric solution (zero points and extinction coefficients) for each night in the B and V bands were determined by a least squares fit to the data. The zero points determined in this way indicate that conditions were photometric throughout the optical observations. The RMS error in the photometric

solution was 0.04 magnitudes in the V and B bands for the October 2003 run and 0.04 and 0.07 for V and B bands respectively in March 2004. The final quoted B and V -band errors in Table 2 include the uncertainty in the fit of the photometric solution and photon statistics added in quadrature.

2.2. Infrared Imaging

Each SofI K_s band integration consisted of a series of co-added 10 second exposures with a random offset within a 40 arcsec jitter box between each exposure. Total on-source integration times ranged between 100 and 5400 seconds (see Table 1). IR data reduction was carried out using Pat Hall’s Infrared Imaging Reduction Software (PHIIRS) which incorporates many standard IRAF routines. We did not follow the usual procedure of obtaining dark frames due to the non-linearity of dark current with incident flux. Instead, we used the PHIIRS task *irsky* to combine individual dithered exposures to simultaneously remove dark current and sky. We used 4–6 frames to construct the sky image for each science exposure; fewer frames were used when the telescope was observing at low airmass, since pupil ghosts produce more severe artifacts when the pupil plane rotates more quickly. These ghosts remained in a few of the final science images, but do not affect the central part of the array where the QSO is located. Flat fielding was done using SofI’s ‘special dome flats’ and custom written reduction script available from the NTT web pages. Registration of the dithered images and median co-addition were done with the PHIIRS routines *irshift* and *ircoadd*, scaling the images to the mode of the sequence. Bright objects were identified in the co-added frame and masked out before running through the co-addition process a second time.

The photometric solution was determined in a manner similar to the optical observations using IR photometric standards from Persson et al. (1998). Although the March 2004 run was photometric, cirrus was present at the end of the October 2003 run. For the affected SofI data, we determined K_s magnitudes by bootstrapping the photometric solution from 2MASS point sources. Typically five 2MASS point sources were available per field for the bootstrap calibration, the larger errors for the magnitudes of these QSOs reflect the RMS in the fit to 2MASS magnitudes³ A filter transformation⁴ was applied in order to place the SofI

³One QSO, B0537–286, was observed during both the October 2003 and March 2004. The magnitude determined from the bootstrap analysis, $K = 16.11 \pm 0.04$ agrees (within the errors) with the magnitude determined under photometric conditions.

⁴<http://www.lis.eso.org/lasilla/sciops/ntt/sofi/setup/ZeroPoint.html>

magnitudes on the Persson K_s system. However, in the absence of contemporaneous J-band magnitudes we have estimated the J–K color as a function of B–K using the dataset of FWW00. Given the scatter in this color-color relation, we expect that the error in assuming a J–K color will affect the filter transformation at < 0.02 magnitudes. The final quoted K_s -band errors in Table 2 include the uncertainty in the fit of the photometric solution, photon statistics and the estimated error in the filter transformation added in quadrature.

Finally, both optical and IR colors were corrected for Galactic extinction according to the maps of Schlegel, Finkbeiner & Davis (1998). Our final optical and IR magnitudes are presented in Table 2.

2.3. Literature Magnitudes

We have supplemented our measurements in Table 2 with magnitudes determined by FWW00, who also achieved near-simultaneous optical and IR (< 6 nights separation) observations of a number of CORALS QSOs. In Table 2 we have corrected the K_n band magnitudes (deduced from the SAAO system) given in FWW00 to K_s magnitudes by using the conversion determined by 2MASS⁵. We also corrected the photometry of FWW00 for Galactic extinction according to the maps of Schlegel et al (1998).

With these supplemental data, we have optical–IR colors for 45/66 program QSOs, with B–K colors for 42. Of these 42, 14 have intervening DLAs; only 3 QSOs with four intervening DLAs were not observed by us or FWW00⁶. The observed sub-sample of CORALS QSOs are representative of the whole sample; only scheduling restrictions prevented the observation of the full sample. In the remainder of this paper we refer the colors determined from our B and K_s magnitudes as B–K.

⁵<http://www.astro.caltech.edu/jmc/2mass/v3/transformations/>

⁶Ellison et al. (2001) reported 19 intervening DLAs. However, one of these, the $z_{\text{abs}} = 1.875$ DLA towards B2314–409 has been shown by Ellison & Lopez (2001) to have an $N(\text{H I})$ slightly below the canonical DLA limit of $2 \times 10^{20} \text{ cm}^{-2}$.

3. Results

3.1. Comparison of Optical and IR Colors

The observed B–K color of a given QSO will change with redshift as the intrinsic spectrum slides through the filter set. Strong emission features such as Ly α and C IV can increase the observed flux in a given band, although flux depression due to the Ly α forest is the dominant source of color shift (e.g. Richards et al. 2003). In Figure 5 we demonstrate this effect by calculating the change in B–K as a function of redshift using the SDSS composite spectrum of Vanden Berk (2001). The color is calculated relative to a reference redshift, in this case $z = 2.3$. We therefore determine a normalized B–K, $(B-K)_n$, which is calculated in the following way. First, we determine the median B–K=2.92 for QSOs in the range $2.2 < z < 2.4$ since the color changes very little over this interval (see Figure 5). Next, we determine a redshift dependent color correction based on the SDSS composite spectrum, displayed graphically in Figure 5. In the case of QSOs with intervening DLAs, we make a correction ($\Delta(B-K)_{DLA}$) for the suppression of flux in the B–band due to the Ly α line. For each DLA, we simulate a spectrum with a damped profile at the redshift z_{abs} and with $N(\text{H I})$ given in Table 3. The spectrum is multiplied by the filter transmission curve and the resulting magnitude compared with an identical spectrum without a DLA absorber. Typical corrections are a few hundredths to a tenth of a magnitude, with a maximum $\Delta(B-K)_{DLA} = 0.18$. The final, normalized B–K color of each QSO is calculated by subtracting the median, the redshift dependent term and (in the case of an intervening DLA) the absorption correction term [$(B-K)_n = (B-K) - 2.92 - f(z) - \Delta(B-K)_{DLA}$].

Table 3 presents the normalized B–K colors for the procedure described above and Figure 6⁷ demonstrates that the resulting color distribution does not exhibit any redshift dependence. There is, however, a large spread in $(B-K)_n$ at any given redshift, regardless of whether or not a DLA is present, as expected for RLQs (e.g. FWW00).

3.2. Limits on Extinction

In order to determine quantitatively whether the colors of QSOs with and without DLAs are drawn from the same distribution, we execute a Kolmogorov-Smirnov (KS) test on two sub-samples: the 14 QSOs with DLAs and 25 without. The KS test yields a 94%

⁷In this Figure, Table 3 and in the following statistics, we only include QSOs whose B and K_s band magnitudes have errors less than 0.3 magnitudes. In practice, this excludes only 3 of the FWW00 QSOs which have poorer photometry. Our conclusions are unaffected by the exclusion of these three.

probability that the two sub-samples are drawn from the same distribution. The mean (median) normalized colors of QSOs with DLAs are +0.12 (+0.01) and –0.10 (+0.02) for QSOs without DLAs with RMS scatters of 0.56 and 0.47 respectively. A student’s T-test yields a test statistic = 1.32, indicating that the mean colors of the two samples are not significantly different.

In order to quantify a limit to the amount of reddening associated with the DLAs in our sample, we run a series of simulations that artificially include/remove reddening in the spectra of QSOs with DLAs. We then calculate the KS statistic compared with the no DLA sample. In each simulation, we redden the observed B–K color of those QSOs with DLAs assuming a fixed $E(B - V)$ for each DLA for both Galactic and SMC extinction curves. We use the parameterizations of SMC ($R_V = 2.93$) and Galactic ($R_V = 3.08$) extinction from Pei (1992) and a second functional fit to Galactic reddening from CCM89, as described in section 1.3. The colors of QSOs without DLAs remain unchanged in these simulations.

To demonstrate how a small change in $E(B - V)$ can affect the color distribution and KS statistic we show the B–K colors for a range of simulations in Figures 7 and 8. The corresponding KS probability is given above each panel. The results of the full simulation gamut for the three extinction curves are shown in Figure 9, where a positive $E(B - V)$ indicates that the spectrum was reddened, whereas a negative value indicates that the effects of dust were removed. These simulations rule out $E(B - V) > 0.04$ (SMC) and $E(B - V) > 0.07$ (MW) at 99% confidence (i.e. KS probability ≤ 0.01 for $E(B - V) < -0.04, -0.07$, with no difference between the Pei and CCM89 Galactic models).

Alternatively, we can consider a reddening that depends on the $N(\text{H I})$ of each DLA. Reddening-to-gas⁸ ratios have been determined in local galaxies, e.g.

$$E(B - V) = \frac{N(\text{HI})}{4.0 \times 10^{22}} \tag{1}$$

for the SMC (Bouchet et al. 1985) and

$$E(B - V) = \frac{N(\text{HI})}{5.8 \times 10^{21}} \tag{2}$$

for the Milky Way (Bohlin, Savage & Drake 1978).

⁸Some authors refer to the relationship between $E(B - V)$ and $N(\text{H I})$ as a dust-to-gas ratio. However, we prefer to use the term reddening-to-gas ratio to avoid confusion with the parameters k and κ that are often used in the literature to denote dust-to-gas ratios inferred, for example, from chemical abundances.

If reddening is removed from the DLA-QSO sample in accordance with the SMC reddening-to-gas relation in Equation 1 the KS probability is 0.39, an inconclusive result. Correcting the colors of QSOs with DLAs using the more extreme Galactic relation in Equation 2 results in colors that are significantly bluer than the no-DLA QSOs, i.e. the reddening correction is too large. The KS probability in this case is 0.03, ruling out a Galactic reddening-to-gas relation at 2σ .

In reality, reddening is likely to be more stochastic than the simple dust recipes adopted here, and extinction curves are likely to vary from DLA to DLA. Our dataset is currently too small to quantify the reddening-to-gas ratios for DLAs through modelling techniques such as χ^2 minimization, although we can rule out a Galactic scaling relation at 97% confidence. However, future work with larger samples, e.g. with DLAs identified from the SDSS, will be able to investigate the reddening-to-gas relation in more detail. Finally, we note that a detailed treatment of other such effects as non-negligible intergalactic medium reddening, host galaxy contributions or exotic extinction laws are beyond the scope of this paper.

3.3. X-ray Observations of the Reddest QSOs

To further investigate the 3 QSOs with the reddest B–K colours, we have searched for archival X-ray observations of these sources. Given a sufficient signal-to-noise in the X-ray data, it is possible to investigate whether ‘intrinsic’ absorption (i.e., associated with the QSO) is present. In principle the X-ray data can measure, or place constraints upon, the integrated hydrogen column along the line of sight (and by assuming a dust-to-gas ratio, on the reddening), as well as the redshift at which the absorption takes place. Since the inferred $N(\text{H I})$ column densities of intrinsic absorbers are frequently an order of magnitude higher than typical intervening DLAs, it is plausible that significant reddening may be induced by such an absorber (although an important caveat is the large possible range in the reddening-to-dust ratios).

Of the three sources with $(\text{B-K})_n > 1$ we found that X-ray observations had been obtained for the QSOs B0438–436 and B0458–020, both of which exhibit DLA absorption. Unfortunately, no X-ray observations have been obtained for B1318–263, the system without a DLA absorber.

B0438–436 has long been known to exhibit significant excess (i.e. above the Galactic contribution) absorption. Evidence for this excess absorption has come from the analysis of ROSAT, ASCA and XMM observations (Serlemitsos et al. 1994; Elvis et al. 1994; Cappi et al. 1997; Brocksopp et al 2004). The best quality data so far are those obtained with

XMM and the best-fit model (Brocksopp et al 2004) is consistent with a solar metallicity absorber with $N(\text{H}) = 1.3 \times 10^{22} \text{ cm}^{-2}$, which Brocksopp et al. assumed to be at the redshift of the QSO⁹. If we assume that ionized and molecular gas is negligible, this column density translates into a $E(B - K) \sim 18.5$ and ~ 5 , for a Galactic and SMC reddening-to-dust ratio respectively and extinction curves from Pei (1992). These values are considerably higher than the $E(B - K)$ observed for this source (see Figure 6). While there are a number of explanations for this discrepancy (e.g. dustless gas near the QSO or AGN extinction curves that are significantly different from Local Group galaxies, e.g. Gaskell et al. 2004) a large reddening due to associated absorption is very plausible.

We have retrieved archival Chandra ACIS data for B0458–020 (ObsID 2985) with a total exposure of 77.76 ksec. The data were analysed in the 0.3–10.0 KeV energy range using CIAO 3.2.1 software and the latest calibration files. B0458–020 suffers from relatively high Galactic absorption, corresponding to $N(\text{H I}) = 7.5 \times 10^{20} \text{ cm}^{-2}$, which hinders the detection of intrinsic absorption which is redshifted to the soft (low energy) part of the spectrum. Indeed, a spectral fit assuming a simple power-law spectrum with only Galactic absorption yields a good fit to the data, i.e. $\chi_{\text{red}}^2 = 0.8$ for 155 degrees of freedom. The best-fit photon index Γ ($f_{\nu} \propto \nu^{\Gamma+1} \text{ ergs s}^{-1} \text{ cm}^{-2}$) was found to be 1.55 ± 0.02 (see Figure 10). The inclusion of absorption at either the QSO or the DLA redshift gave no significant improvement to the fit: $N(\text{H}) < 2 \times 10^{21} \text{ cm}^{-2}$ with 99% confidence (F-test statistics $F \sim 0.002$ for $\Delta\chi^2 \sim 7.3$ and 1 additional parameter). Using the Pei (1992) extinction laws this corresponds to an upper limit $E(B - K) < 2.8$ and < 0.7 , for a Galactic and SMC reddening-to-dust ratio if the absorber is located in the host galaxy. Associated absorption could therefore be the cause of the red color of this QSO, although better X-ray data would be required to confirm this. However, we note that Carilli et al. (1998) found that 80% of red QSOs in their sample exhibited strong 21 cm absorption at the QSO redshift, supporting the view that red colors may be often caused by intrinsic absorption.

4. Discussion

In a series of papers, Fall & Pei (1989), Fall, Pei & McMahon (1989) and Pei, Fall & Bechtold (1991) investigated whether the spectral indices of QSOs with DLAs were systematically steeper than QSOs with no intervening galaxy. In particular, in the latter of these

⁹With sufficiently high quality data, it is possible to determine the absorption redshift. However, associated absorption is often the working assumption since the column densities greatly exceed that of typical intervening absorbers. In this case, the intervening DLAs has $N(\text{H I}) = 6 \times 10^{20} \text{ cm}^{-2}$.

papers, new data with higher spectrophotometric accuracy were obtained and a sample of 66 QSOs analysed for reddening. The distribution of spectral indices in the DLA sample (20 QSOs) was found to differ at the 99.999% confidence level from the no-DLA (46 QSOs) sample. The inferred dust:gas ratio was 5–20% of that in the Milky Way. Further support for observed reddening was reported by Outram et al. (2001) who found redder B–R colors for QSOs with $0.5 < z < 1.5$ high equivalent width Mg II absorbers. The inferred color excess was $E(B - V) \sim 0.04$. More recently, Wild & Hewett (2005) have found a convincing reddening signature associated with low z Ca II absorbers in the SDSS, although still at a modest level: $E(B - V) = 0.06$. Individual cases of DLA reddening have been reported based either on differential reddening in lensed systems (e.g. Zuo et al. 1997 for a DLA at $z_{\text{abs}} = 1.4$) or the detection of the 2175 Å graphite feature (Junkkarinen et al. 2004 for a DLA at $z_{\text{abs}} = 0.5$). However, some caution is required when comparing inferences on dust extinction at different redshift ranges since the amount, source and composition of dust may differ, for example as the dominant source of dust shifts from Type II supernovae to lower mass stars (e.g. Hirashita et al. 2005). Nonetheless, these works apparently provide robust evidence for the systematic reddening of QSOs with intervening absorption systems at both high and low redshifts.

Recently, however, Murphy & Liske (2004) re-visited the spectral fitting approach with a large statistical sample drawn from the SDSS. In addition to its size (~ 1450 QSOs, with 72 DLAs) this sample has the advantage that its data acquisition is homogeneous and the spectral indices are fit over a wider wavelength range than was done in earlier work. With these improvements, Murphy & Liske (2004) found no steepening of the spectral indices for QSOs with DLAs and determined a limit of $E(B - V) < 0.02$ (99% confidence). Although Murphy & Liske adopt a similar approach to Fall, Pei and collaborators in fitting spectral indices, they do so with an order of magnitude larger sample, wider wavelength coverage and uniform data acquisition. Since QSOs have a wide range of intrinsic colors and spectral shapes, using the broadest baseline possible is important for identifying a systematic dust reddening.

For the first time, optical–IR colors can now contribute to the on-going debate. Although our sample is modest in size in comparison with the SDSS (although comparable with the samples of Pei, Fall and collaborators), the broad wavelength coverage provides significant leverage for detecting reddening. For example, whereas the B–K color changes by 0.74 for an $E(B - V)=0.05$ (SMC extinction $z_{\text{em}} = 3.0, z_{\text{abs}} = 2.6$), the $B - R$ color changes only by 0.35. Moreover, the sample of QSOs on which we conduct this work is based on an optically complete survey of radio-loud quasars. Therefore, our sample of DLAs should not be subject to selection effects associated with dust extinction.

Our results are presented graphically in Figure 6 where we show the normalized B–K colors for QSOs with and without DLAs. The mean color of QSOs without DLAs is -0.10 , compared with $+0.12$ for the DLA sub-sample. Both color distributions have RMS scatters ~ 0.5 . Neither a student’s T-test nor a KS test find any significant difference in the B–K colors of the two sub-samples. We determine a 3σ limit of $E(B - V) < 0.04, 0.07$ for SMC and Galactic extinction respectively based on the results of our KS test simulations. Although not quite as sensitive as limits from the SDSS (Murphy & Liske 2004), our sample is optically complete and could potentially contain heavily extinguished QSOs which would not have been found in magnitude limited samples. However, the low $E(B - V)$ allowed by this work shows that even in optically complete samples, the amount of reddening is small. Such low values of $E(B - V)$ are consistent with the small H_2 fractions observed in DLAs; whilst a handful of absorbers have $\log f(H_2) \sim -2$, most have $\log f(H_2) < -5$ (Ledoux, Petitjean & Srianand 2003). Indeed, Tumlinson et al. (2002) have shown that low molecular fractions are common in Galactic and Magellanic Cloud sightlines when $E(B - V) \lesssim 0.08$.

Although this work has not found any indication that QSOs are significantly reddened by intervening DLAs, evidence that *some* dust is present in DLAs is well established from the abundances of refractory versus volatile elements such as Cr and Zn (e.g. Pettini et al. 1994, 1997). Akerman et al. (2005) have obtained Zn and Fe abundances for many of the DLAs in our sample; we reproduce these abundance results in Table 3 adopting the solar reference values from Lodders (2003). Vladilo & Péroux (2005) have recently suggested that reddening will increase linearly with $N(\text{Zn})$ and become especially severe when $\log N(\text{Zn}) > 13.2$. In Figure 11 we plot the normalized B–K color versus $N(\text{Zn})$ using the column densities reported in Akerman et al. (2005)¹⁰. We detect no trend between normalized color and $\log N(\text{Zn})$, although we have only 3 DLAs with $\log N(\text{Zn}) > 13.0$. Nonetheless, Akerman et al (2005) find that the mean weighted metallicity of CORALS DLAs is only marginally higher (although consistent within the error bars) than previous samples.

In Figure 12 we investigate whether there is any correlation between $N(\text{H I})$ or depletion (as measured by $[\text{Fe}/\text{Zn}]$) and reddening. The two reddest QSOs which also show DLA absorption have slightly larger than average ($[\text{Fe}/\text{Zn}] = -0.3$, Prochaska & Wolfe 2002), but still modest depletions. The rest of the sample (including two systems with comparable depletions to the reddest DLA-harboring QSOs) do not show any correlation between depletion and reddening. Similarly, the $N(\text{HI})$ of one of the three very red QSOs in our sample has the

¹⁰We make the usual assumption that Zn II is the dominant ionization stage of this element and that the contribution from other ionization stages is negligible. Moreover, in Figures 11 and 12 we include 2 DLAs within 3000 km s^{-1} of the QSO, plus one further absorber whose $N(\text{H I})$ is just below the canonical DLA limit.

DLA with the highest $N(\text{H I})$ amongst CORALS absorbers. However, a second high $N(\text{H I})$ DLA has apparently not reddened its background QSO to a similar extent and the reddest QSO with a DLA has only a modest $N(\text{H I})$. Overall, there is no obvious trend between $(B-K)_n$ and $N(\text{H I})$. On the other hand, Khare et al. (2004) *do* report tentative evidence for a correlation between the inferred $E(B - V)$ (based on broad band SDSS colors) and $[\text{Cr}/\text{Zn}]$ (analogous to the $[\text{Fe}/\text{Zn}]$ plotted in Figure 12). However, the Khare et al. result is based on the two systems in their sample with $[\text{Cr}/\text{Zn}] < 1$, and only one of the DLAs in our sample may have such a high dust:gas ratio. The normalized B–K color of this QSO is mildly redder than the median color of the other QSOs, although this can certainly not be taken as evidence for a correlation between depletion and reddening. It would be of great interest to further investigate the correlation between reddening and dust:gas ratio in a larger sample of objects.

Prantzos & Boissier (2000) have suggested that dust bias is responsible for the observed anti-correlation between $[\text{Zn}/\text{H}]$ and $N(\text{H I})$, and propose an empirical ‘dust filter’, i.e. that DLAs in optically selected samples all have $\log N(\text{H I}) + [\text{Zn}/\text{H}] < 21$. In Figure 13 we plot $N(\text{H I})$ versus $[\text{Zn}/\text{H}]$ from the compilation of DLAs in Kulkarni et al. (2005); the dust filter suggested by Prantzos & Boissier (2000) is shown by the dashed line. We can combine the suggested cut-off of $\log N(\text{H I}) + [\text{Zn}/\text{H}] < 21$ with a reddening-to-gas ratio which scales with metallicity in order to calculate what $E(B - V)$ is implied. For example, it is straightforward to show that if the Galactic reddening-to-gas ratio given in Eqn 2 is scaled by $[\text{Zn}/\text{H}]$ and satisfies the criterion $\log N(\text{H I}) + [\text{Zn}/\text{H}] < 21$, then $E(B - V) < 0.17$. This is the $E(B-V)$ value required to ensure that no high $N(\text{HI})$, high $[\text{Zn}/\text{H}]$ systems are observed; $E(B - V) = 0.17$ is indeed considerably larger than the limits determined by this work and that of Murphy & Liske (2004). We can alternatively calculate where the observed cut-off in Figure 13 would lie for a given assumed $E(B - V)$. For example, an $E(B - V) < 0.05$ implies $\log N(\text{H I}) + [\text{Zn}/\text{H}] < 20.46$ (again using Equation 2 scaled by $10^{[\text{Zn}/\text{H}]}$); this cut-off is shown in Figure 13 by a dot-dash line. If future work determines an $E(B - V) \ll 0.05$, it may (depending on the assumed reddening-to-gas ratio) become difficult to quantitatively reconcile the $N(\text{H I})$ - $[\text{Zn}/\text{H}]$ distribution with dust bias.

In Figure 13 we also plot the $N(\text{H I})$ and $[\text{Zn}/\text{H}]$ values for the CORALS DLAs, which should not be subject to dust bias. The figure shows that CORALS DLAs are not distinguishable from other (literature) DLAs in terms of their $N(\text{H I})$ - $[\text{Zn}/\text{H}]$ distribution. Moreover, they do not lie above the empirical cut-off which has been proposed to be due to dust. However, in the chemical evolution models of Churches et al.(2004), $\lesssim 9\%$ of DLAs (depending on the choice of spin parameter) are expected to be in this ‘dust forbidden’ region (A. Nelson, 2005, private communication). It therefore seems premature at this point to interpret the lack of high $N(\text{H I})$, metal-rich CORALS DLAs as evidence that the anti-correlation is not

caused by dust.

If future work concludes that dust *is* the reason for the anti-correlation in Figure 13, then the locus of data points compared with the theoretical lines and the lack of high CORALS values may indicate that typical $E(B - V)$ values are simply intrinsically low in most DLAs. Indeed, Ellison, Kewley & Mallen-Ornelas (2005) found $E(B - V) \lesssim 0.2$ even in the central parts of absorber counterparts at $z < 0.5$. Alternatively, the implied $E(B - V)$ values from this and the work of Murphy & Liske (2004) may be explained if the dust extinction is relatively grey, as been proposed to explain the $E(B - V)$ values observed towards some gamma-ray burst hosts (e.g. Vreeswijk et al. 2004).

One of the greatest uncertainties in this work is the unknown nature (i.e. composition, grain size and, therefore, extinction curve) of dust in damped systems. The main observational distinction between SMC and Galactic extinction curves (with the LMC being somewhat intermediate between the two, see Figure 1) is the presence of a 'bump' at 2175 Å, attributed to graphite. A handful of detections of this feature at cosmological redshifts exist associated with 3 Mg II absorbers with $z_{\text{abs}} \sim 1.5$ in the SDSS (Wang et al. 2004), a high N(HI) DLA at $z_{\text{abs}} \sim 0.5$ (Junkkarinen et al. 2004) and several cases of galaxy lenses (e.g. Falco et al. 1999; Toft et al. 2000; Motta et al. 2002; Wucknitz et al. 2003; Munoz et al. 2004). However, gravitationally lensed systems are clearly special cases since the impact parameter through the galaxy is necessarily small. Malhotra (1997) have claimed to see the 2175 Å feature in stacked (non-lensed) QSO spectra exhibiting Mg II absorption, although stacks of SDSS spectra have failed to reproduce this (M. Murphy, 2005, private communication; Menard 2005; Khare et al. 2005; Wild & Hewett 2005). Although further investigation is warranted, this may be evidence that Galactic dust is not generally applicable for absorbers towards unlensed QSOs. Theoretical models of dust in high redshift galaxies enriched by high mass Type II SN may be more relevant than local extinction curves. However, the extinction properties amongst these models also vary tremendously depending on progenitor mass and mixing (e.g. Hirashita et al. 2005).

5. Conclusions

In this work we have investigated whether dust in DLAs can cause a significant, systematic reddening of background QSOs by obtaining B–K colors for an optically complete, radio-selected quasar sample. We determine normalized colors which account for redshift dependence (analogous to a K-correction which accounts for Ly α flux decrement and emission lines) and suppressed B-band flux due to DLA absorption. The mean normalized B–K color of the DLA sub-sample is 0.12 ± 0.56 , compared with -0.10 ± 0.47 for the no-DLA sub-sample.

Both a student’s T-test and KS test indicate that there is no statistical difference between the distribution of B–K colors in the two sub-samples. We place a limit on the amount of reddening that may be present, by correcting the colors of QSOs with DLAs using a range of $E(B - V)$ values. Adopting an SMC extinction curve, we place a 3σ limit on the systematic reddening: $E(B - V) < 0.04$, assuming a fixed reddening for each DLA. In general, there is no correlation between depletion, $N(\text{Zn})$ or $N(\text{H I})$ and reddening. Finally, we have searched for archival X-ray data of the three reddest QSOs in our sample in order to test whether their extreme $(B-K)_n$ colors maybe due to intrinsic (i.e. at $z \sim z_{\text{em}}$) absorption. Of these three QSOs, two have data available, and the spectrum of one (B0438–436) shows evidence for a high $N(\text{H I})$ absorber associated with the QSO which may be the cause of the very red color.

These results support relatively low extinctions towards high redshift DLAs, and agree with the $E(B - V)$ values inferred from the optically selected SDSS work of Murphy & Liske (2004). Therefore, although a handful of individual absorbers may cause more severe reddening (e.g. Junkkarinen et al. 2004), these seem to be the exception rather than the rule. A number of observational works have also inferred relatively small reddening at lower redshifts (e.g. Khare et al. 2005; Menard 2005; Wild & Hewett 2005). Combined with previous work which has found that the number density and gas content of intervening absorbers (Ellison et al. 2001, 2004) and their metallicities (Akerman et al. 2005) are not largely different from samples whose optical completeness exceeds $B \sim 19$, it seems increasingly unlikely that dust bias has severely skewed our view of high redshift DLAs. Put another way, the red(dened) QSO population is unlikely to be linked to dust in high redshift DLAs.

The authors would like to thank the ever expert help of the La Silla observatory staff, especially Valentin Ivanov. SLE is grateful to Jon Willis for providing advice regarding the reduction of the SofI data presented here. We are also grateful to Paul Francis for making the data presented in FWW00 available in electronic format and for additional information on that dataset. SLE also acknowledges informative discussions with Michael Murphy and is grateful for his feedback on an earlier draft of this work. PL acknowledges financial support by Fondecyt’s grant 1040719. This publication makes use of data products from the Two Micron All Sky Survey, which is a joint project of the University of Massachusetts and the Infrared Processing and Analysis Center/California Institute of Technology, funded by the National Aeronautics and Space Administration and the National Science Foundation. This work also made use of the NASA Extragalactic Database (NED).

REFERENCES

- Akerman, C. J., Ellison, S. L., Pettini, M., Steidel C. C., 2005, *A&A*, submitted
- Barkhouse, W., & Hall, P. B., 2001, *AJ*, 121, 2843
- Benn, C. R., Vigotti, M., Carballo, R., Gonzalez-Serrano, J. I., Sanchez, S. F., 1998, *MNRAS*, 295, 451
- Bohlin, R. C., Savage, B. D., Drake, J. F., 1978, *ApJ*, 224, 132
- Bouchet, P., Lequeux, J., Maurice, E., Prevot, M. L., Prevot-Burnichon, M. L., 1985, *A&A*, 149, 330
- Bregman, J. N., Glassgold, A. E., Huggins, P. J., Lebofsky, M. J., Rieke, G. H., Aller, M. F., Aller, H. D., Hodge, P. E., 1981, *Nature*, 293, 714
- Brooksopp, C., Puchnarewicz, E. M., Mason, K. O., Cordova, F. A., Priedhorsky, W. C., 2004, *MNRAS*, 349, 687
- Cappi, M.; Matsuoka, M.; Comastri, A.; Brinkmann, W.; Elvis, M.; Palumbo, G. G. C.; Vignali, C., 1997, *ApJ* 478 492
- Cardelli, J. A., Clayton, G. C., & Mathis, J. S., 1989, *ApJ*, 345, 245
- Carilli, C. L., Menten, K. M., Reid, M. J., Rupen, M. P., Yun, M., 1998, *ApJ*, 494, 175
- Churches, D. K., Nelson, A. H., & Edmunds, M. G., 2004 *MNRAS*, 347, 1234
- Draine, B. T., 2003, *ARA&A*, 41, 241
- Drinkwater, M., Wiklind, T., & Combes, F., 1996, *A&A*, 312, 771
- Ellison, S. L., Churchill, C. W., Rix, S. A., Pettini, M., 2004, *ApJ*, 615, 118
- Ellison, S. L., Kewley, L. J., & Mallén-Ornelas, G., 2005, *MNRAS*, 357, 354
- Ellison, S. L., & Lopez, S., 2001, *A&A*, 380, 117
- Ellison, S. L., Yan, L., Hook, I., Pettini, M., Wall, J., Shaver, P., 2001, *A&A*, 379, 393
- Elvis, M., Fiore, F., Wilkes, B., McDowell, J., Bechtold, J., 1994, *ApJ* 422 60
- Falco, E. E., et al., 1999, *ApJ*, 523, 617
- Fall, S. M., Pei, Y., 1993, *ApJ*, 402, 479

- Fall, S. M., Pei, Y., McMahon, R. G., 1989, *ApJ*, 341, L5
- Francis, P., Whiting, M., & Webster, R., 2000, *PASA*, 17, 56
- Gaskell, C. M., Goosmann, R. W., Antonucci, R. R. J., Whysong, D. H., 2004, *ApJ*, 616, 147
- Glikman, E., Gregg, M. D., Lacy, M., Helfand, D. J., Becker, R. H., White, R. L., 2004, *ApJ*, 607, 60
- Gregg, M. D., Wisotzki, L., Becker, R. H., Maza, J., Schechter, P. L., White, R. L., Brotherton, M. S., Winn, J. N., 2000, *AJ*, 119, 2535
- Hirashita, H., Nozawa, T., Kozasa, T., Ishii, T. T., Takeuchi, T. T., *MNRAS*, 2005, accepted
- Hopkins et al., 2004, *AJ*, 128, 1112
- Hutchings, J. B., Giasson, J., 2001, *PASP*, 113, 1205
- Junkkarinen, V. T., Cohen, R. D., Beaver, E. A., Burbidge, E. M., Lyons, R. W., Madejski, G., 2004, *ApJ*, 614, 658
- Khare, P., Kulkarni, V. P., Lauroesch, J. T., York, D. G., Crofts, A. P. S., Nakamura, O., 2004, *ApJ*, 616, 86
- Khare, P., IAUC 199, "Probing Galaxies through Quasar Absorption Lines," eds. Williams, Shu, Menard, astro-ph/0504532
- Kulkarni, V., Fall, S. M., Lauroesch, J. T., York, D. G., Welty, D. E., Khare, P., Truran, J., W., 2005, *ApJ*, 618, 68
- Landolt, A., 1992, *AJ*, 104, 340
- Ledoux, C., Petitjean, P., Srianand, R., 2003, *MNRAS*, 346, 209
- Lodders, K., 2003, *ApJ*, 591, 1220
- Malhotra, S., 1997, *ApJ*, 488, L101
- Mathis, J. S., 1990, *ARA&A*, 28, 37
- Menard, B., 2005, IAUC 199, "Probing Galaxies through Quasar Absorption Lines," eds. Williams, Shu, Menard.
- Meyer, D. M., & Roth, K. C., 1990, *ApJ*, 363, 57

- Meyer, D. M., & York D. G. 1992, ApJ, 399, 121
- Motta, V., Mediavilla, E., Munoz, J. A., Falco, E., Kochanek, C. S., Arribas, S., Garcia-Lorenzo, B., Oscoz, A., Serra-Ricart, M., 2002, ApJ, 574, 719
- Munoz, J. A., Falco, E. E., Kochanek, C. S., McLeod, B. A., Mediavilla, E., 2004, ApJ, 605, 614
- Murphy, M. T., & Liske, J., 2004, MNRAS, 345, L31
- Nestor, D. B., Turnshek, D. A., Rao, S. M., 2005, ApJ, accepted
- Pei, Y., 1992, ApJ, 395, 130
- Pei, Y., Fall, S. M., 1995, ApJ, 454, 69
- Pei, Y., Fall, S. M., Bechtold, J., 1991, ApJ, 378, 6
- Pei, Y., Fall, S. M., Hauser, M. G., 1999, ApJ, 552, 604
- Persson, S. E., Murphy, D. C., Krzeminski, W., Roth, M., Rieke, M. J., 1998, AJ, 116, 2475
- Pettini, M., Smith, L.J., King, D.L., & Hunstead, R.W. 1997, ApJ, 486, 665
- Pettini, M., Smith, L.J., Hunstead, R.W., King, D.L., 1994, ApJ, 426, 79
- Prantzos, N., Boissier, S., 2000, MNRAS, 315, 82
- Prochaska, J. X., & Wolfe, A. M. 2002, ApJ, 566, 68
- Rawlings, S., Lacy, M., Sivia, D. S., Eales, S. A., 1995 MNRAS, 274, 428
- Richards, G. T., et al., 2003, AJ, 126, 1131
- Serlemitsos, P., Yaqoob, T., Ricker, G., Woo, J., Kunieda, H., Terashima, Y., 1994, PASJ, 46, L43
- Schlegel, D.J., Finkbeiner, D.P., & Davis, M. 1998 ApJ, 500, 525
- Smith, H. E., & Spinrad, H., 1980, ApJ, 236, 419
- Smith, J. A., et al., 2002, AJ, 123, 2121
- Stein, W. A., & Sitko, M. L., 1984, AJ, 89, 1688

- Stern, D., Hall, P. B., Barrientos, L. F., Bunker, A. J., Elston, R., Ledlow, M. J., Raines, S. N., Willis, J., 2003, *ApJ*, 596, 39
- Toft, S., Hjorth, J., & Burud, I., 2000, *A&A*, 357, 115
- Tumlinson, J., et al., 2002, *ApJ*, 566, 857
- Vanden Berk, D. E., et al. 2001, *ApJ*, 122, 549
- Vladilo, G. & Péroux, C., 2005, *A&A*, submitted
- Vreeswijk, P., et al., 2004, *A&A*, 419, 927
- Wang, J., Hall, P. B., Ge, J., Li, A., Schneider, D., 2004, *ApJ*, 609, 589
- Wild, V., & Hewett, P. C., 2005, *MNRAS*, in press
- Webster, R. L., Francis, P. J., Peterson, B. A., Drinkwater, M. J., Masci, F. J., 1995, *Nature*, 375, 469
- White, R. L., Helfand, D. J., Becker, R. H., Gregg, M. D., Postman, M., Lauer, T. R., Oegerle, W., 2003, *AJ*, 126, 706
- Whiting, M., Webster, R., & Francis, P., 2001, *MNRAS*, 323, 718
- Wucknitz, O., Wisotzki, L., Lopez, S., Gregg, M. D., 2003, *A&A*, 405, 445
- Zuo, L., Beaver, E. A., Burbidge, E. M., Cohen, R. D., Junkkarinen, V. T., Lyons, R. W., *ApJ*, 477, 568

Table 1. Target List and Observing Journal

QSO	z_{em}	Observing Run	Integration Time SofI (s)	Integration Time SuSI2 (s)	SuSI2 Filter
B0113–283	2.555	Oct 2003	1800	200	B
B0122–005	2.280	Oct 2003	300
B0244–128	2.201	Oct 2003	300	40	B
B0256–393	3.449	Oct 2003	4320	360	V
B0325–222	2.220	Oct 2003	300	150	B
B0329–255	2.685	Oct 2003	200	40	B
B0335–122	3.442	Oct 2003	4500	360	V
B0347–211	2.944	Oct 2003	...	800	B
B0405–331	2.570	Oct 2003	600	60	B
B0420+022	2.277	Oct 2003	800	100	B
B0422–389	2.346	Oct 2003	300	40	B
B0432–440	2.649	Oct 2003	800	100	B
B0434–188	2.702	Oct 2003	1800	200	B
B0438–436	2.863	Oct 2003	800	100	B
B0451–282	2.560	Oct 2003	300	60	B
B0458–020	2.286	Oct 2003	1200	200	B
B0528–250	2.765	Oct 2003	300	60	B
B0537–286	3.110	Mar 2004	1800	200	B
				200	V
B0610–436	3.461	Oct 2003	300	60	V
B0919–260	2.300	Mar 2004	300	60	B
B0933–333	2.906	Mar 2004	1800	200	B
				200	V
B1010–427	2.954	Mar 2004	800	20	B
				20	V
B1055–301	2.523	Mar 2004	800	100	B
B1136–156	2.625	Mar 2004	800	200	B
B1147–192	2.489	Mar 2004	4500	360	B
B1149–084	2.370	Mar 2004	1800	200	B

Table 1—Continued

QSO	z_{em}	Observing Run	Integration Time SofI (s)	Integration Time SuSI2 (s)	SuSI2 Filter
B1228–113	3.528	Mar 2004	4920	800	B
				800	V
B1228–310	2.276	Mar 2004	1800	200	B
B1230–101	2.394	Mar 2004	1800	200	B
B1256–243	2.263	Mar 2004	800	100	B
B1318–263	2.027	Mar 2004	4500	800	B
B1351–018	3.710	Mar 2004	...	800	B
B1354–107	3.006	Mar 2004	300	60	B
				60	V
B1402–012	2.518	Mar 2004	300	20	B
B1418–064	3.689	Mar 2004	4500	360	B
				360	V
B2311–373	2.476	Oct 2003	300	40	B

Table 2. CORALS QSO magnitudes

QSO	z_{em}	B_{JUKST}	B	V	K	Ref
B0017–307	2.666	20.0
B0039–407	2.478	19.7
B0104–275	2.492	19.3
B0113–283	2.555	19.6	19.64±0.04	...	17.32±0.15	This work
B0122–005	2.280	17.9	15.75±0.03	This work
B0244–128	2.201	18.4	18.21±0.04	...	15.13±0.10	This work
B0256–393	3.449	20.6	...	19.32±0.04	16.78±0.04	This work
B0325–222	2.220	19.0	19.37±0.04	...	16.44±0.04	This work
B0329–255	2.685	17.6	18.11±0.04	...	16.00±0.15	This work
B0335–122	3.442	20.6	...	20.11±0.04	17.51±0.18	This work
B0347–211	2.944	20.5	20.89±0.04	This work
B0405–331	2.570	19.1	19.41±0.04	...	16.28±0.04	This work
B0420+022	2.277	19.7	19.17±0.04	...	16.37±0.04	This work
B0422–389	2.346	18.4	19.11±0.04	...	16.60±0.13	This work
B0432–440	2.649	19.9	19.81±0.04	...	17.37±0.04	This work
B0434–188	2.702	18.8	19.25±0.04	...	16.24±0.07	This work
B0438–436	2.863	19.4	20.68±0.04	...	16.09±0.03	This work
B0451–282	2.560	18.0	18.22±0.04	...	15.35±0.03	This work
B0458–020	2.286	...	19.33±0.04	...	15.32±0.03	This work
B0528–250	2.765	18.1	18.16±0.04	...	15.46±0.03	This work
B0537–286	3.110	20.0	19.84±0.07	19.06±0.04	16.16±0.03	This work
B0601–172	2.711
B0610–436	3.461	18.5	...	18.85±0.04	14.43±0.03	This work
B0819–032	2.352
B0834–201	2.752
B0913+003	3.074	20.9
B0919–260	2.300	...	18.05±0.07	...	15.04±0.03	This work
B0933–333	2.906	...	19.72±0.07	19.39±0.04	16.71±0.04	This work
B1010–427	2.954	...	17.25±0.07	16.61±0.03	15.31±0.03	This work
B1055–301	2.523	19.3	19.36±0.07	...	16.35±0.03	This work
B1136–156	2.625	19.1	19.31±0.07	...	16.26±0.03	This work

Table 2—Continued

QSO	z_{em}	B_{JUKST}	B	V	K	Ref
B1147–192	2.489	20.3	20.38 ± 0.07	...	17.08 ± 0.04	This work
B1149–084	2.370	20.0	19.70 ± 0.07	...	16.52 ± 0.04	This work
B1228–113	3.528	21.5	20.85 ± 0.07	19.48 ± 0.04	16.66 ± 0.03	This work
B1228–310	2.276	19.8	19.36 ± 0.07	...	16.79 ± 0.04	This work
B1230–101	2.394	19.6	19.73 ± 0.07	...	16.99 ± 0.04	This work
B1251–407	4.464
B1256–243	2.263	19.4	19.45 ± 0.07	...	16.36 ± 0.03	This work
B1318–263	2.027	21.3	21.37 ± 0.07	...	17.57 ± 0.03	This work
B1351–018	3.710	21.5	21.00 ± 0.07	This work
B1354–107	3.006	18.4	19.00 ± 0.07	18.15 ± 0.04	15.70 ± 0.03	This work
B1402–012	2.518	18.0	18.50 ± 0.07	...	15.63 ± 0.03	This work
B1406–267	2.430
B1418–064	3.689	20.5	20.42 ± 0.07	18.97 ± 0.04	16.58 ± 0.03	This work
B1430–178	2.331	19.4	18.82 ± 0.07	18.67 ± 0.06	15.68 ± 0.23	FWW00
B1535+004	3.497
B1556–245	2.813	...	18.46 ± 0.06	18.69 ± 0.06	16.53 ± 0.31	FWW00
B1635–035	2.871	...	20.06 ± 0.32	19.83 ± 0.20	17.36 ± 0.32	FWW00
B1701+016	2.842
B1705+018	2.575	...	18.30 ± 0.07	18.07 ± 0.06	15.85 ± 0.10	FWW00
B1937–101	3.780
B2000–330	3.780	...	18.34 ± 0.06	17.05 ± 0.05	15.05 ± 0.08	FWW00
B2126–158	3.275	17.1	17.63 ± 0.05	16.66 ± 0.05	14.27 ± 0.05	FWW00
B2149–307	2.330	18.4	17.89 ± 0.05	17.67 ± 0.05	15.21 ± 0.13	FWW00
B2212–299	2.703	17.4	17.41 ± 0.05	17.31 ± 0.05	14.58 ± 0.06	FWW00
B2215+020	3.550	22.0	21.61 ± 0.31	20.24 ± 0.10	19.30 ± 1.78	FWW00
B2224+006	2.248	22.0
B2245–059	3.295	19.7
B2245–328	2.268	18.3	19.00 ± 0.07	18.76 ± 0.07	16.08 ± 0.19	FWW00
B2256+017	2.663	19.6
B2311–373	2.476	18.4	18.99 ± 0.04	...	16.38 ± 0.04	This work
B2314–340	3.100	18.3

Table 2—Continued

QSO	z_{em}	B_{JUKST}	B	V	K	Ref
B2314–409	2.448	19.0	18.26 ± 0.06	18.03 ± 0.05	15.58 ± 0.08	FWW00
B2315–172	2.462	21.0
B2325–150	2.465	20.0
B2351–154	2.665	18.7	18.82 ± 0.07	18.60 ± 0.06	16.37 ± 0.26	FWW00

Table 3. Normalized Colors and Intervening Absorber Properties for CORALS QSOs with Near-Simultaneous B–K Colors

QSO	z_{em}	z_{abs}	N(HI)	$(B - K)_n$	[Zn/H]	[Fe/H]	Abundance Ref.
B0113–283	2.555	-0.49 ± 0.16
B0244–128	2.201	0.17 ± 0.11
B0325–222	2.220	0.02 ± 0.06
B0329–255	2.685	-0.68 ± 0.16
B0405–331	2.570	2.570	20.60	0.28 ± 0.06	< -0.49	-1.74	Akerman et al. (2005)
B0420+022	2.277	-0.12 ± 0.06
B0422–389	2.346	-0.42 ± 0.14
B0432–440	2.649	2.297	20.78	-0.41 ± 0.06	< -1.21	-1.45	Akerman et al. (2005)
B0434–188	2.702	0.21 ± 0.08
B0438–436	2.863	2.347	20.78	1.54 ± 0.05	-0.68	-1.30	Akerman et al. (2005)
B0451–282	2.560	0.07 ± 0.05
B0458–020	2.286	2.039	21.65	1.02 ± 0.05	-1.15	-1.61	Akerman et al. (2005)
B0528–250	2.765	2.141	20.75	-0.28 ± 0.05	-1.45	-1.57	Akerman et al. (2005)
		2.811	21.20		-0.47	-1.11	Akerman et al. (2005)
B0537–286	3.110	2.974	20.30	0.35 ± 0.08	< -0.40	Akerman et al. (2005)
B0919–260	2.300	0.09 ± 0.08
B0933–333	2.906	2.682	20.48	-0.06 ± 0.08	< -1.12	-1.54	Akerman et al. (2005)
B1010–427	2.954	-1.14 ± 0.08
B1055–301	2.523	1.904	21.54	0.16 ± 0.08	-1.26	-1.57	Akerman et al. (2005)
B1136–156	2.625	0.28 ± 0.08
B1147–192	2.489	0.42 ± 0.08
B1149–084	2.370	0.25 ± 0.08
B1228–113	3.528	2.193	20.60	0.19 ± 0.08	-0.22	Akerman et al. (2005)
B1228–310	2.276	-0.35 ± 0.08
B1230–101	2.394	1.931	20.48	-0.20 ± 0.08	-0.17	-0.63	Akerman et al. (2005)
B1256–243	2.263	0.17 ± 0.08
B1318–263	2.027	1.02 ± 0.08
B1354–107	3.006	2.501	20.40	0.08 ± 0.08	< -1.32	-1.25	Akerman et al. (2005)
		2.966	20.78		< -1.48	-1.54	Akerman et al. (2005)
B1402–012	2.518	0.02 ± 0.08
B1418–064	3.689	3.449	20.40	-0.43 ± 0.08	< -1.04	-1.72	Akerman et al. (2005)

Table 3—Continued

QSO	z_{em}	z_{abs}	N(HI)	$(B - K)_n$	[Zn/H]	[Fe/H]	Abundance Ref.
B1430–178	2.331	0.21 ± 0.24
B1705+018	2.575	-0.34 ± 0.12
B2000–330	3.780	-1.16 ± 0.10
B2126–158	3.275	-0.20 ± 0.07
B2149–307	2.330	-0.25 ± 0.14
B2212–299	2.703	0.03 ± 0.08
B2245–328	2.268	0.00 ± 0.20
B2311–373	2.476	2.182	20.48	-0.32 ± 0.06	< -1.29	-1.70	Akerman et al. (2005)
B2314–409	2.448	1.857	20.90	-0.23 ± 0.10	-1.02	-1.33	Ellison & Lopez (2001)
		1.875	20.10		< -1.19	-1.88	Ellison & Lopez (2001)
B2351–154	2.665	-0.34 ± 0.27

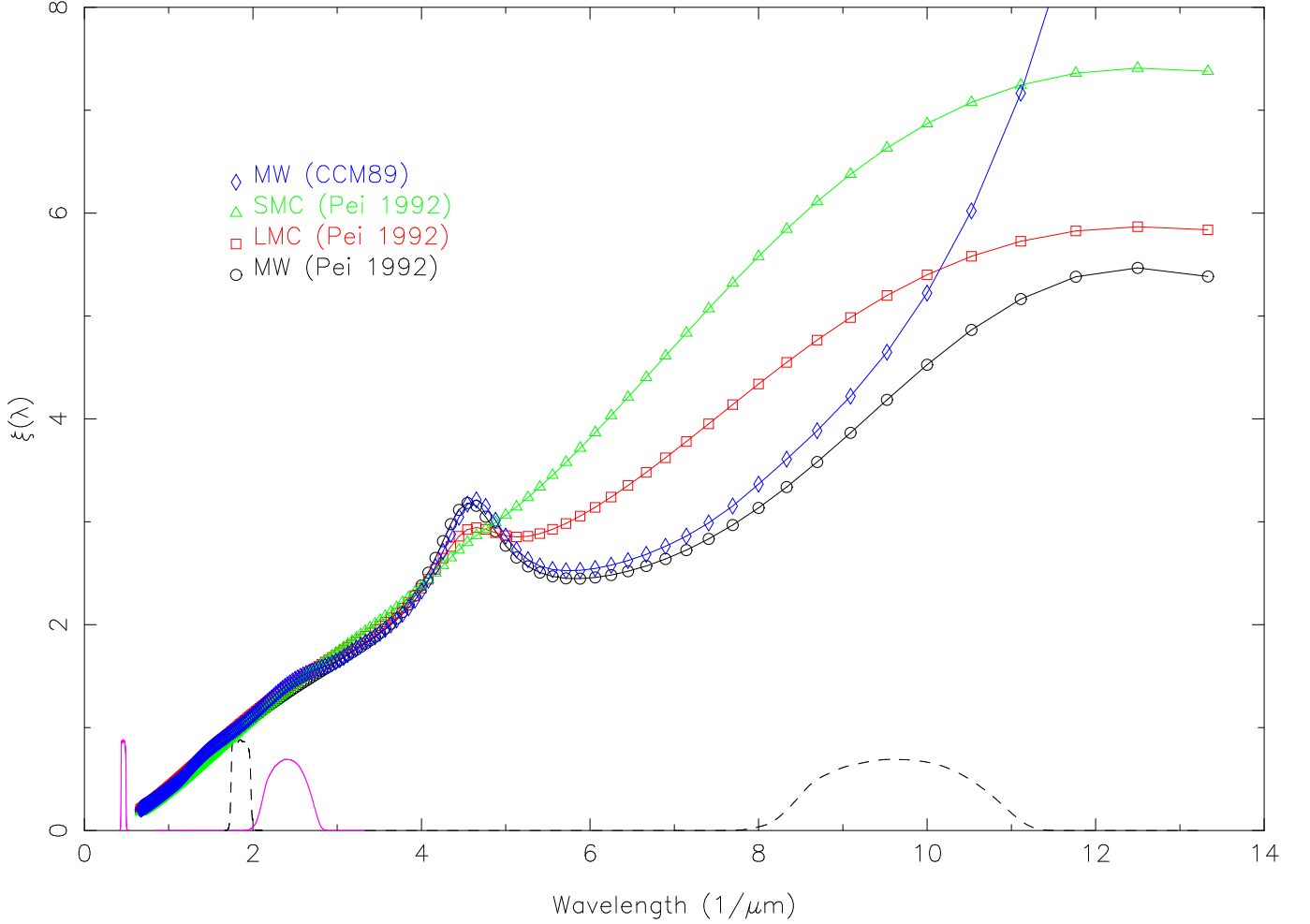


Fig. 1.— Extinction curves for the parameterizations of Pei (1992) and Cardelli, Clayton & Mathis (1989). Assumed R_V values are 2.93 (SMC), 3.16 (LMC) and 3.08 (MW). There were no data available at wavelengths $\leq 1000 \text{ \AA}$, hence the divergence in the FUV for the Galactic curves represents an extrapolation of the fitting functions. Filter transmission curves along the base of the plot illustrate what rest wavelengths correspond to the B and K_s bands for $z = 0$ (solid) and $z = 3$ (dashed).

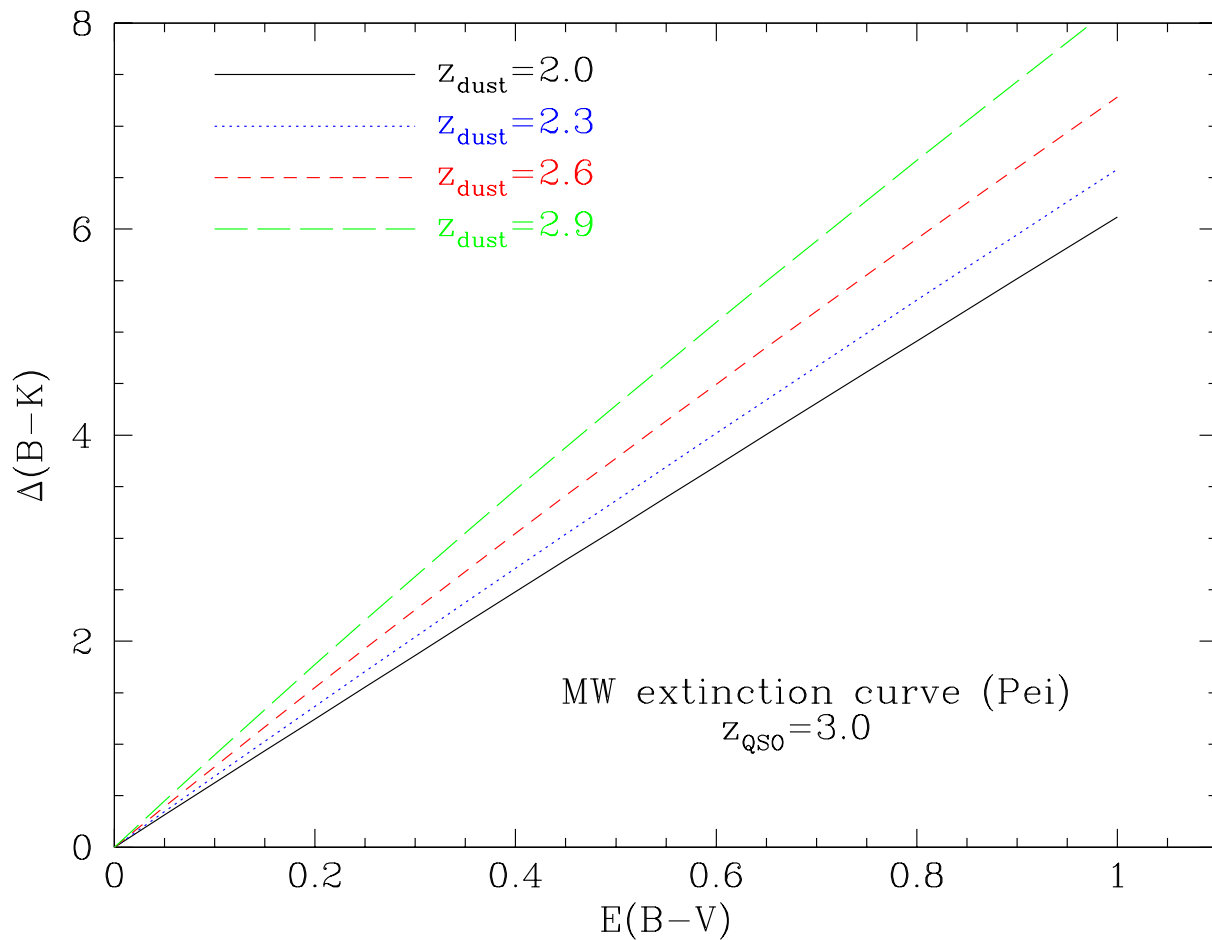


Fig. 2.— Theoretical reddening of a $z_{\text{em}} = 3.0$ QSO with an intervening absorber at $z_{\text{abs}} = 2.0, 2.3, 2.6, 2.9$. We assume a Galactic extinction curve based on the parameterization of Pei (1992).

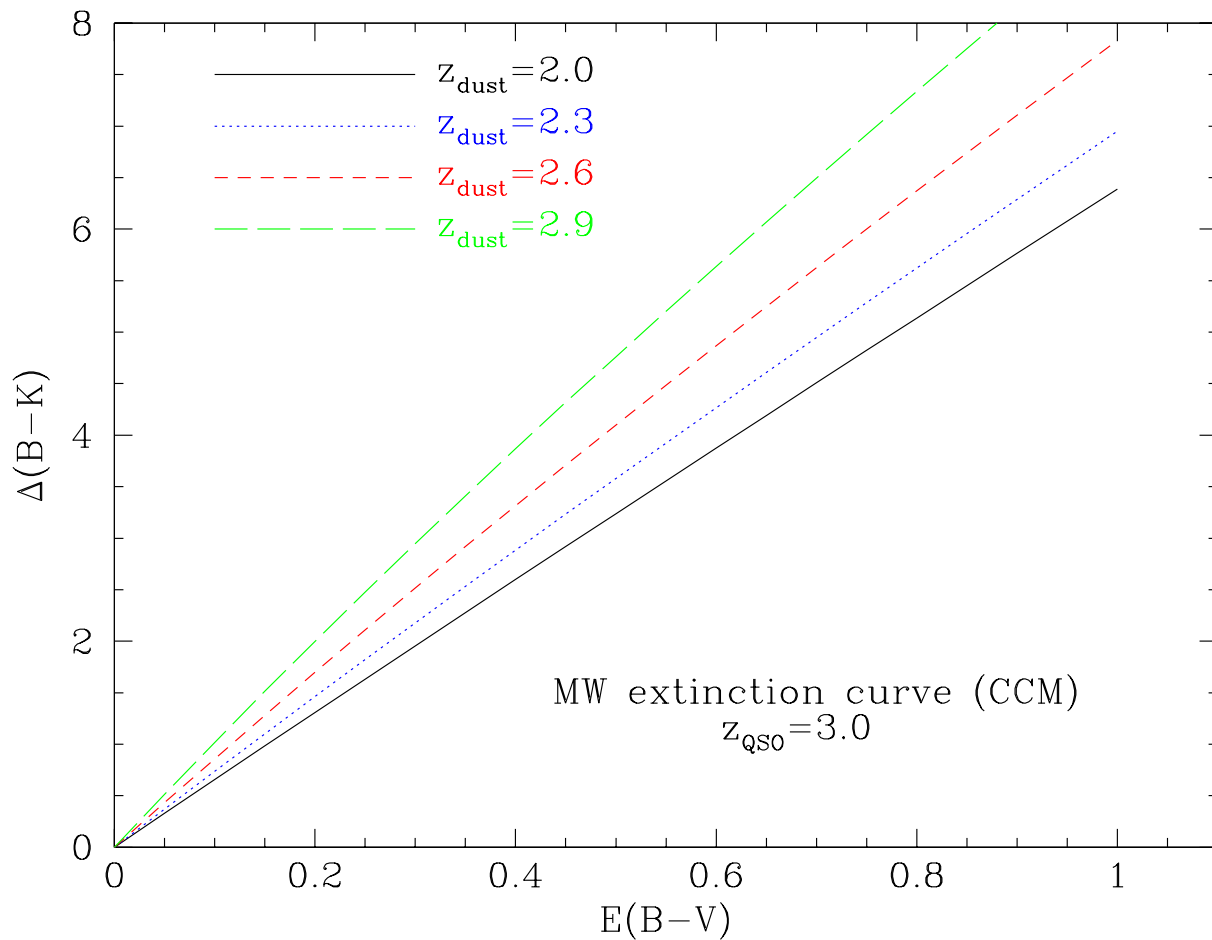


Fig. 3.— Theoretical reddening of a $z_{\text{em}} = 3.0$ QSO with an intervening absorber at $z_{\text{abs}} = 2.0, 2.3, 2.6, 2.9$. We assume a Galactic extinction curve based on the parameterization of Cardelli, Clayton & Mathis (1989) with $R_V = 3.08$.

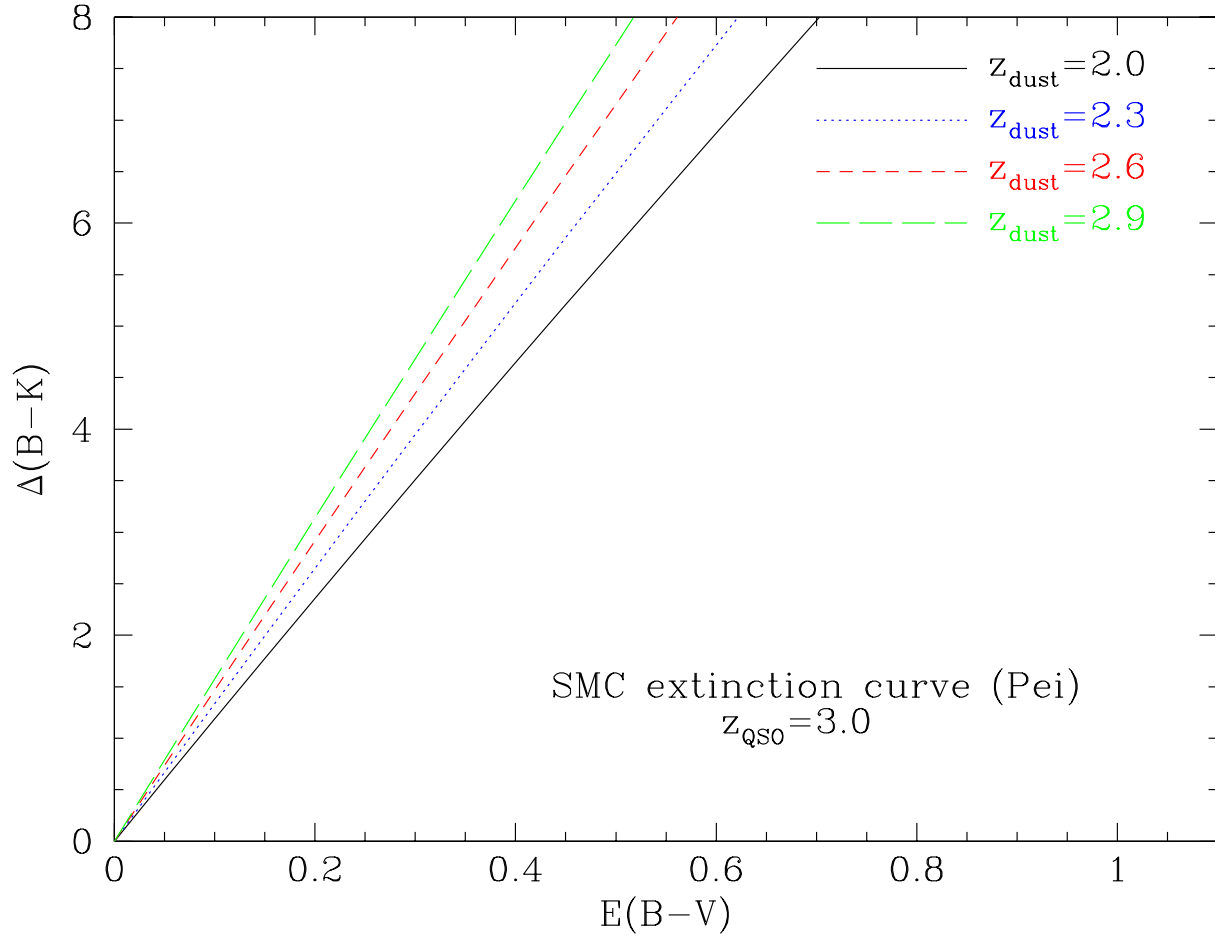


Fig. 4.— Theoretical reddening of a $z_{\text{em}} = 3.0$ QSO with an intervening absorber at $z_{\text{abs}} = 2.0, 2.3, 2.6, 2.9$. We assume an SMC extinction curve based on the parameterization of Pei (1992).

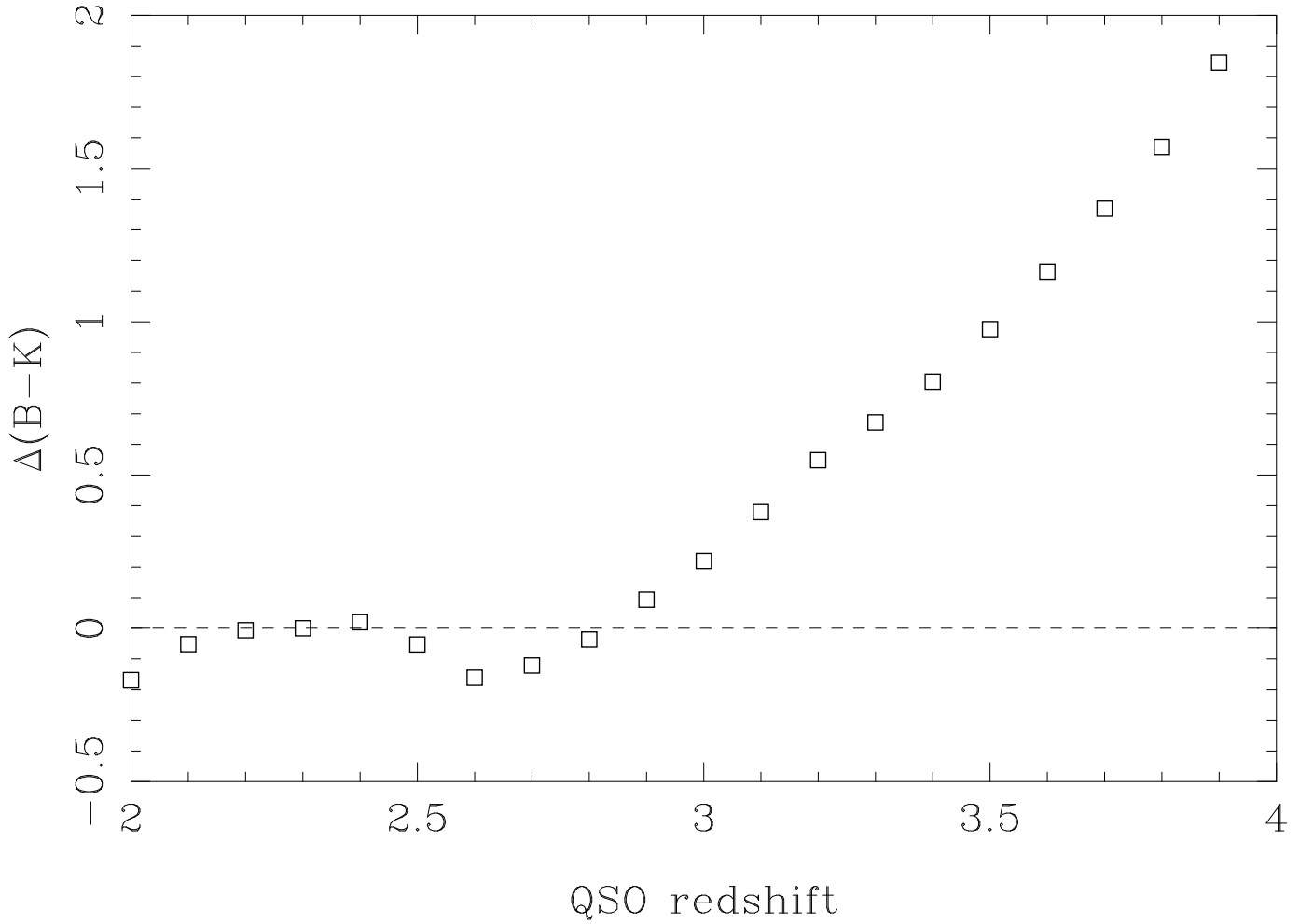


Fig. 5.— Change in B–K color as a function of redshift determined using the SDSS composite spectrum of Vanden Berk (2001). Color changes are relative to $z = 2.3$.

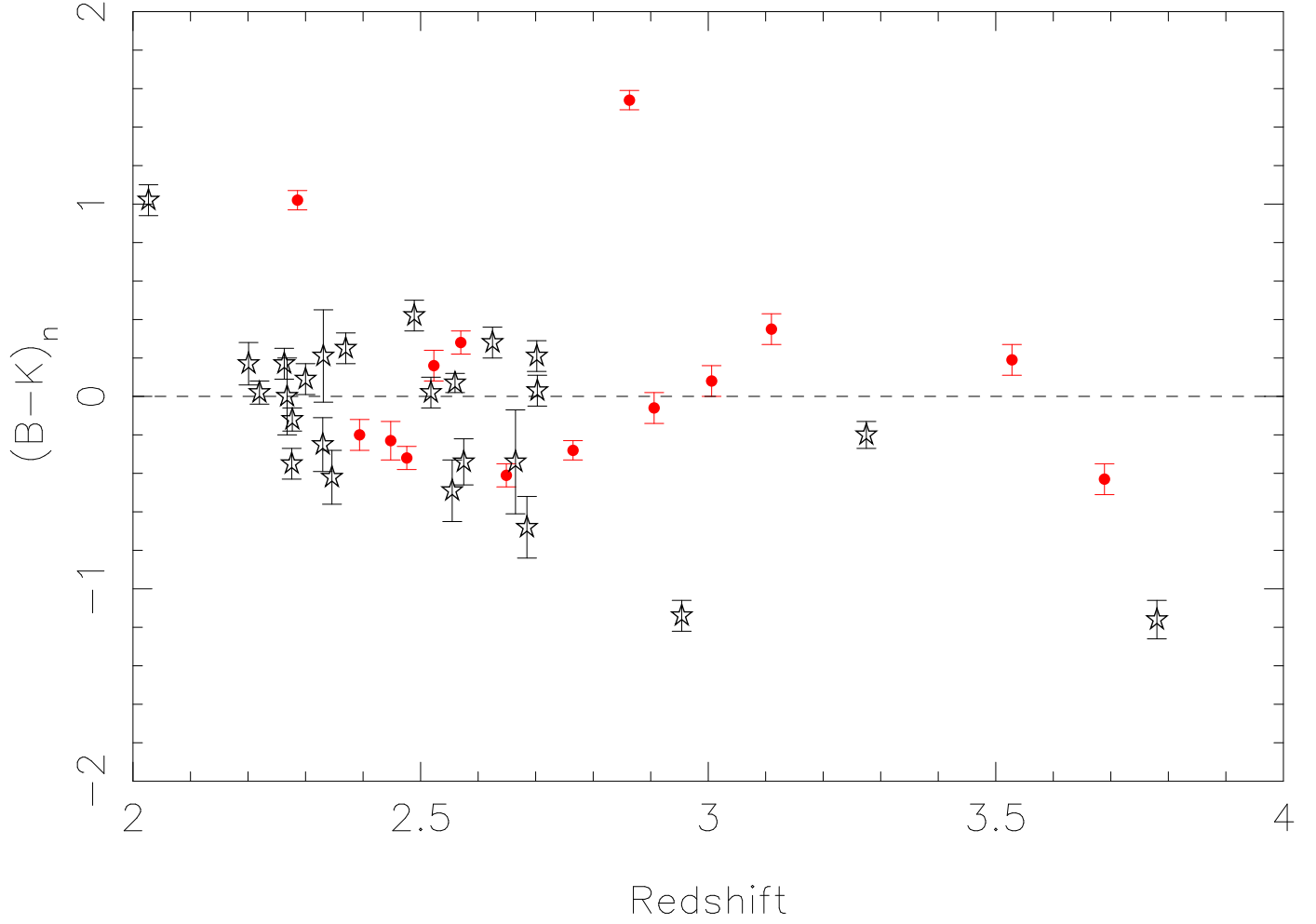


Fig. 6.— Redshift distribution of normalized B–K colors for QSOs with (filled circles) and without (open stars) DLAs.

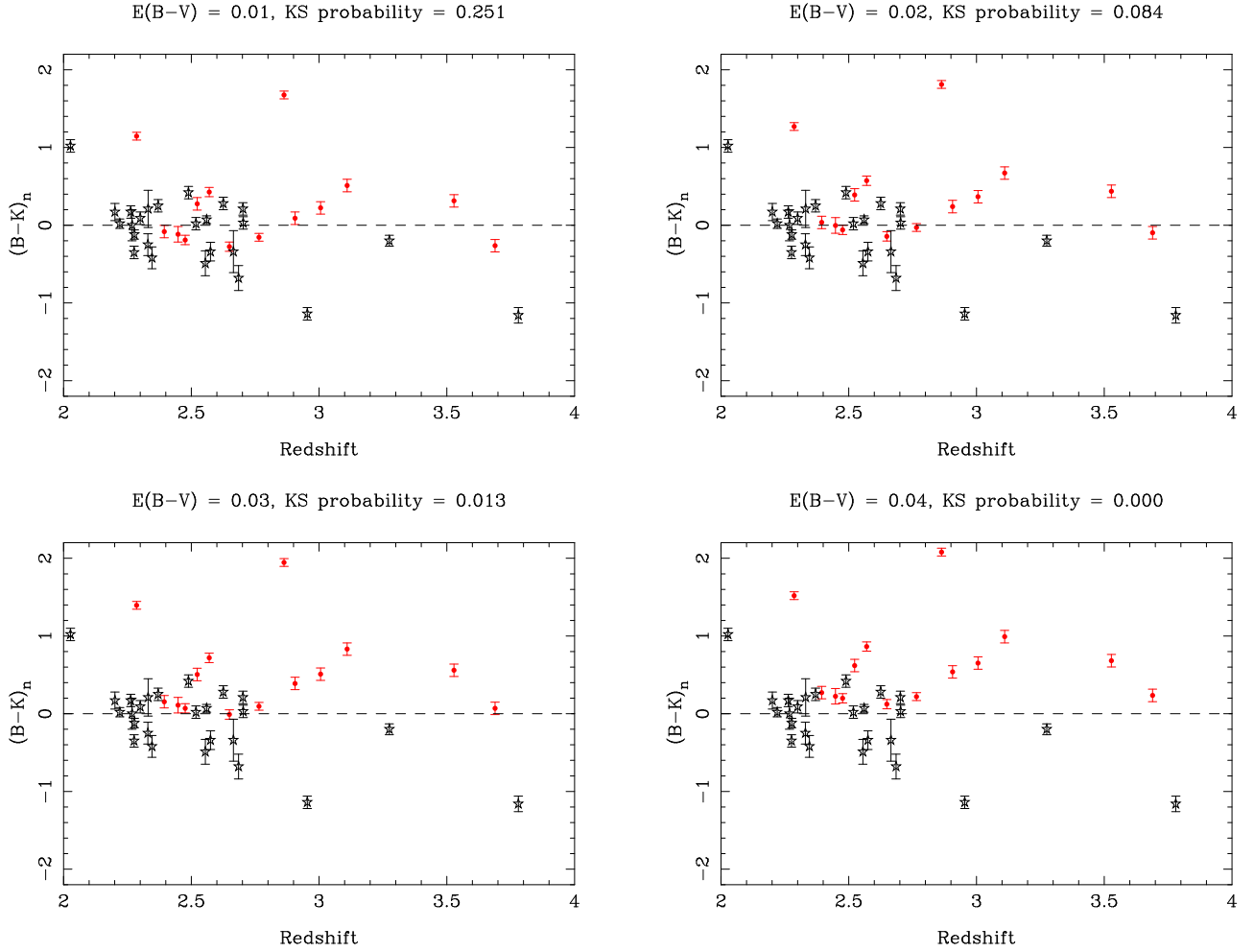


Fig. 7.— Redshift distribution of normalized B–K colors for QSOs with (filled circles) and without (open stars) DLAs with reddening *added* to the former population assuming a Pei (1992) SMC extinction law. Each of the four panels illustrates a different degree of reddening and shows the KS probability that the DLA and non-DLA QSOs are drawn from the same color distribution.

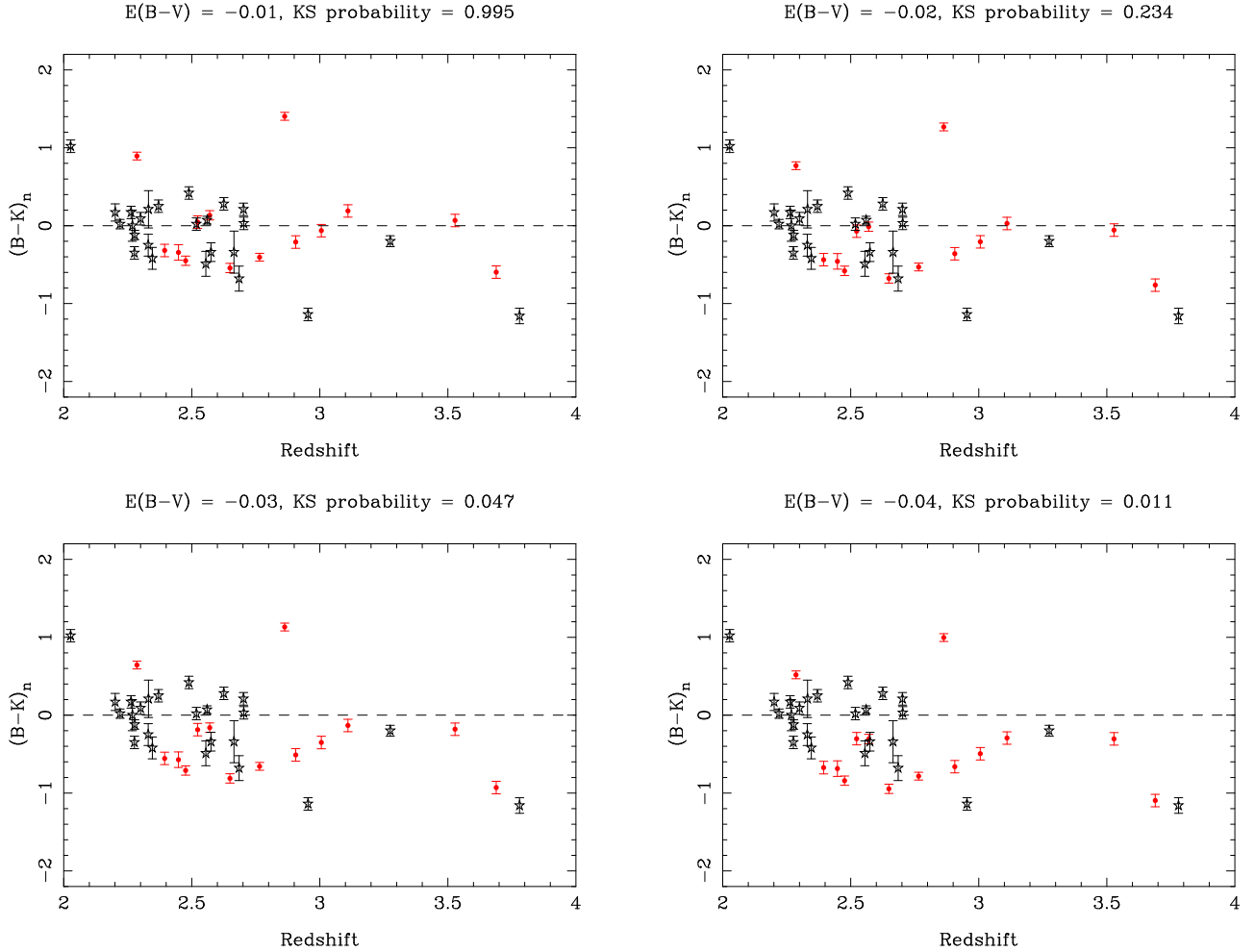


Fig. 8.— Redshift distribution of normalized B–K colors for QSOs with (filled circles) and without (open stars) DLA reddening *removed* to the former population assuming a Pei (1992) SMC extinction law. Each of the four panels illustrates a different degree of reddening and shows the KS probability that the DLA and non-DLA QSOs are drawn from the same color distribution.

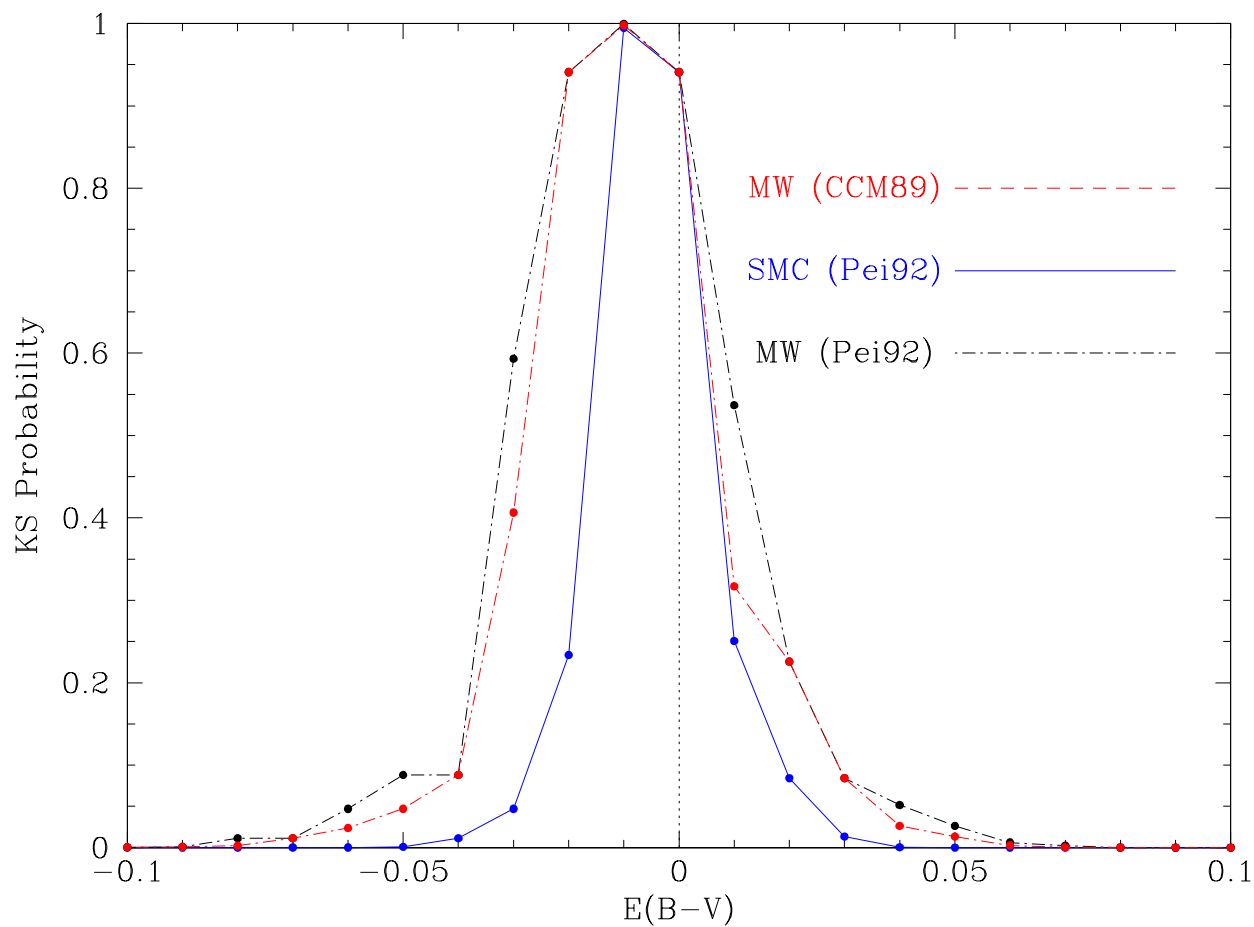


Fig. 9.— KS probability that the $(B-K)_n$ colors of QSOs with and without DLAs are drawn from the same distribution, for simulations which include reddening in the former population. Positive values of $E(B - V)$ indicate that the effect of dust (i.e. reddening) was added to the simulated spectra and negative values indicate that the effect of dust was removed. The vertical dotted line indicates that the raw $(B-K)_n$ have been used, i.e. no reddening included.

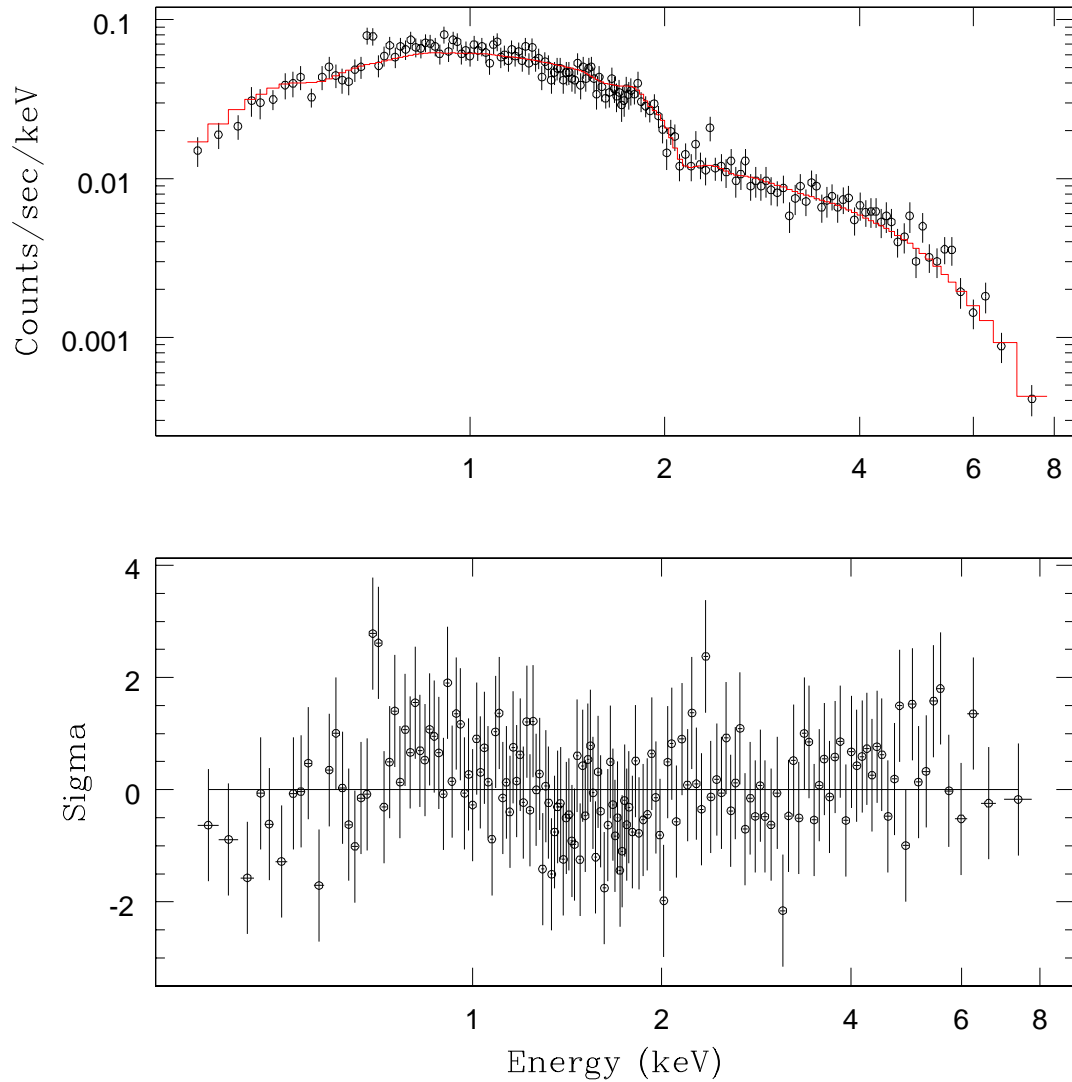


Fig. 10.— Best-fit χ^2 plots of the B0458–020 Chandra observations. The fit and sigma ((data - model) / error) plots are shown after convolving with the instrument response (top and bottom panels, respectively). The data were fitted with a single power-law model absorbed by a Galactic foreground $N(\text{H I})$ column (thin continuous line in top panel).

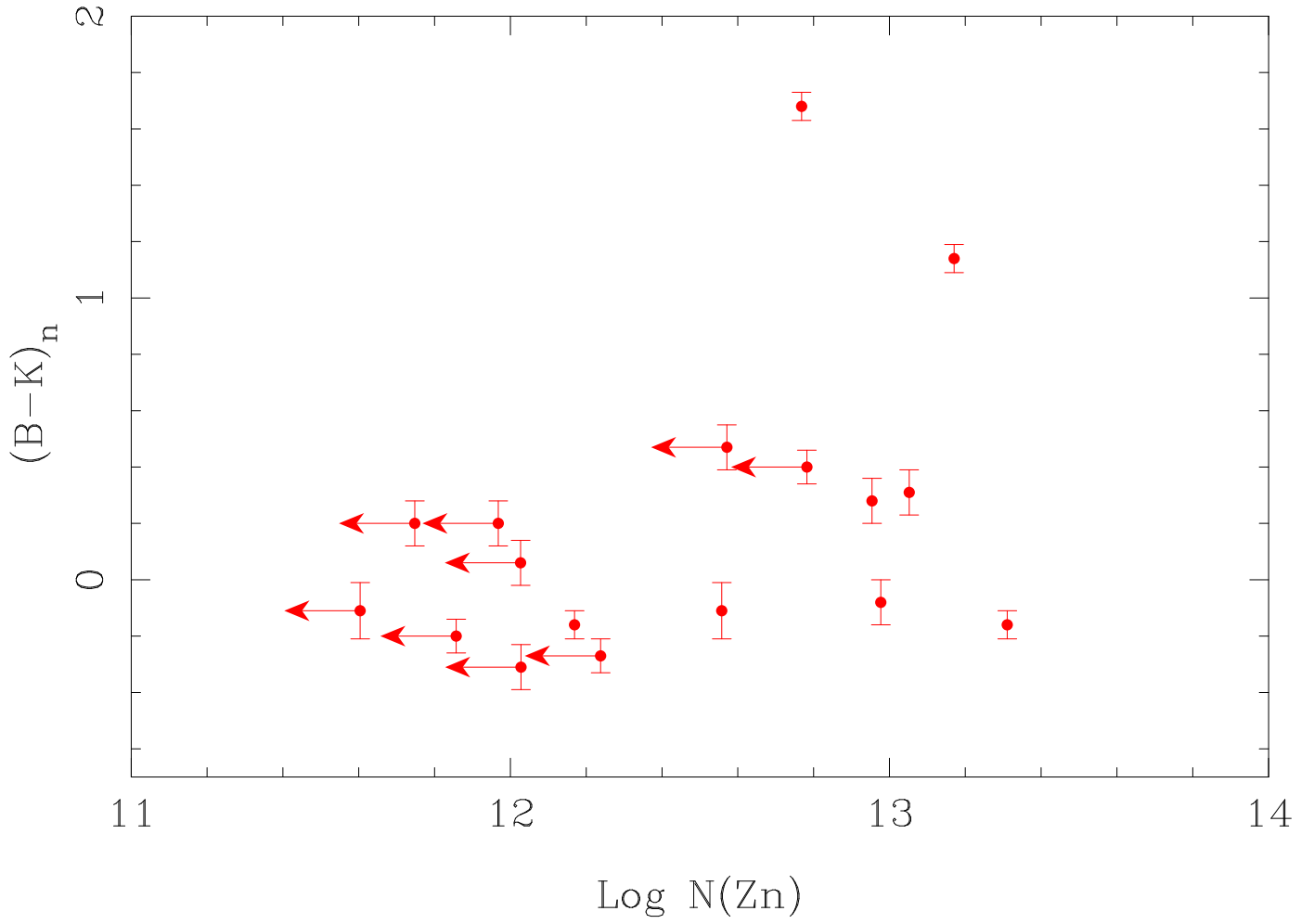


Fig. 11.— Normalized B–K color of CORALS DLAs as a function of Zn column density.

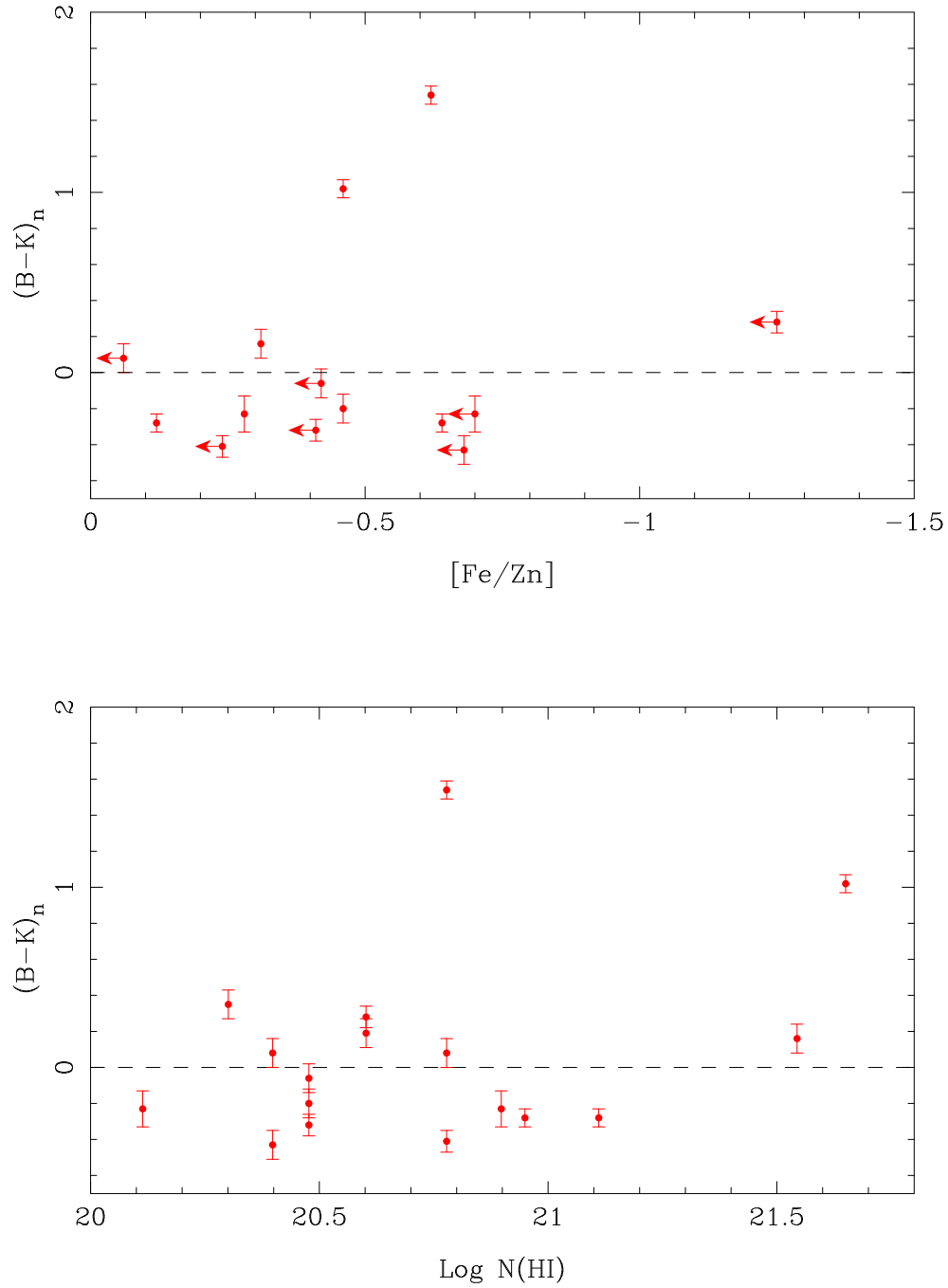


Fig. 12.— Top panel: Normalized B–K color as a function of depletion, as measured by $[Fe/Zn]$. Bottom panel: Normalized B–K color as a function of neutral hydrogen column density, $N(\text{HI})$.

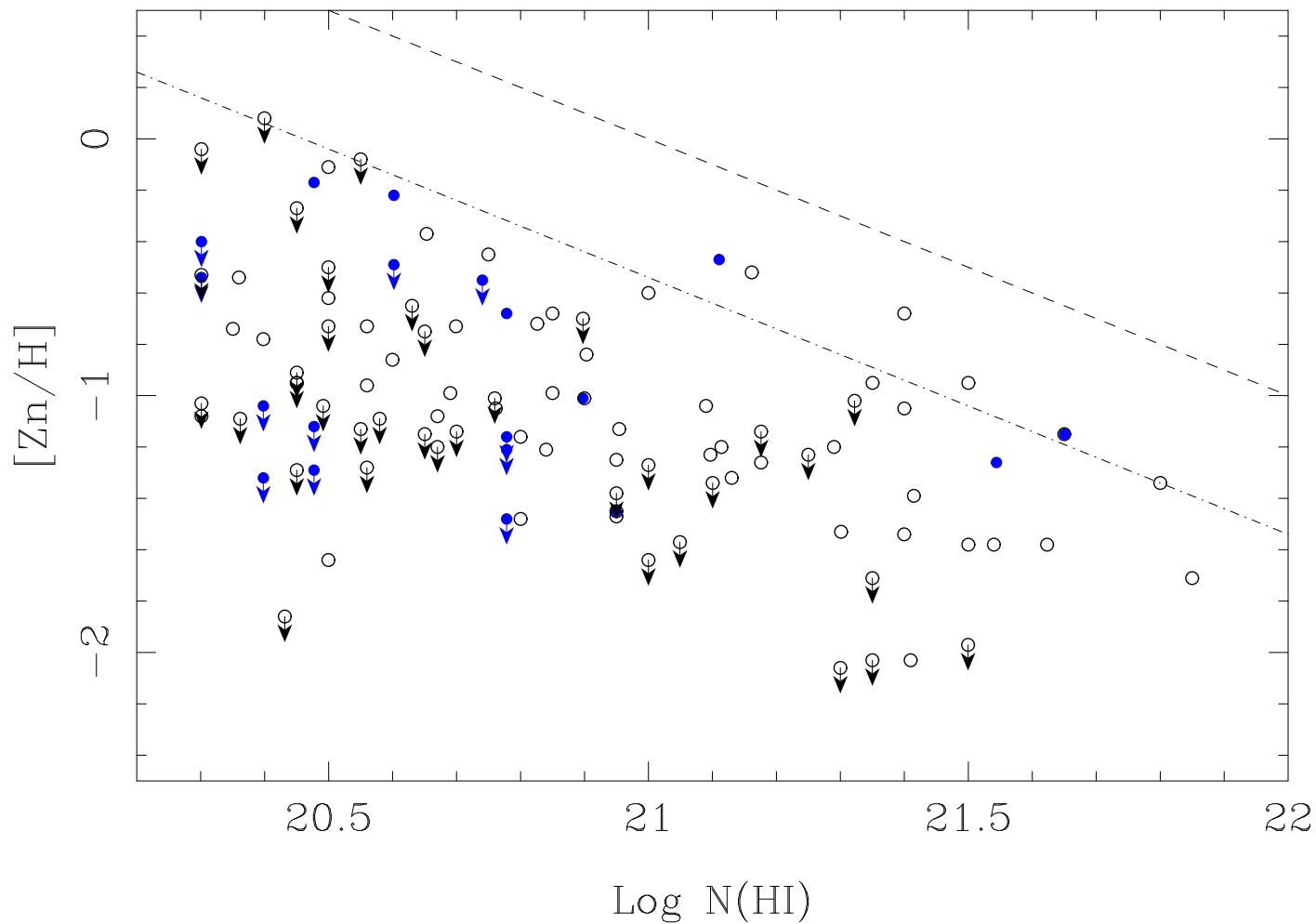


Fig. 13.— Metallicity versus $N(\text{H I})$ column density for DLAs taken from the compilation of Kulkarni et al. (2005) and for the CORALS DLAs (Akerman et al. 2005), shown by open and filled circles respectively. The dashed line shows the proposed ‘dust filter’ of Prantzos & Boissier (2000): $\log N(\text{H I}) + [\text{Zn}/\text{H}] < 21$, which corresponds to $E(B - V) < 0.17$ for a Galactic gas-to-reddening law scaled by metallicity. The dot-dashed line shows where the cut-off would lie if $E(B - V) < 0.05$, i.e. $\log N(\text{H I}) + [\text{Zn}/\text{H}] < 20.46$.